Final Report for AOARD Grant FA2386-11-1-4055

Opto-Electronically Efficient Conjugated Polymers by Stress-Induced Molecular Constraints

July 15, 2012

Name of Principal Investigators: Arnold Chang-Mou Yang
- e-mail address : acyang@mse.nthu.edu.tw
- Institution : Department of Materials Science and Engineering, National Tsing Hua University, Hsinchu, Taiwan
- Mailing Address : 101, Kuang Fu Road, Hsinchu City, Taiwan
- Phone : +886 (3) 572 0792
- Fax : +886 (3) 572 2366

Period of Performance: 07/01/2011 – 06/30/2012

Abstract: The dramatic enhancement of optoelectronic efficiencies of conjugated polymers induced by segmental stresses recently discovered by our group was further studied in various fundamental facets of this important property in addition to some major breakthrough in the road for real applications. In details, the influences of chain conformations influenced by molecular stresses were investigated in the single-molecule systems of MEH-PPV brushes and pancakes grafted on silane-primed substrates. The dramatic plunge in electric conductivity of the polymer P3HT confined in mesoscopic dimensions was investigated in the light of molecular constraints, and a Mott's hopping model that included the electron-phonon couplings was constructed to explain and reveal the details of the molecular stress effects. Single molecules of P3HT dispersed in PS were stretched to study the stress-enhancement effect on the crystallizing conjugated polymers. The effects of molecular flows triggered in thin film dewetting were further studied to reveal the mechanisms of chain stretching. Further to the thin film instability, the dewetting was activated by stress transfer from a thin film stored with large residual stress to result huge enhancement of the optoelectronic efficiencies. All these experiments patch a coherent picture of the stress-induced optoelectronic efficiencies by the mechanism of electron-phonon interactions. Along with the efficiency increases, the exciton quenching arising from the effect of a pulling electric field diminished, indicating that the suppression of electron-phonon interactions in the stress-rigidified molecular segments had altered the fundamental processes of exciton formation and annihilation. Furthermore, accompanying the efficiency enhancement, the life of conjugated polymer was found to increase. Finally, the efficiency enhancement can be produced in solid films of conjugated polymers using simple imprints under good control over the molecular deformation; a patent was filed based on this revelation.

1. Photoluminescence of Single-Molecule Brushes and Pancakes of Conjugated Polymer MEH-PPV of Stress-Influenced Conformations

Single molecule poly[2-methoxy-5-(2'-ethylhexyl)oxy)-1,4-phenylenevinylene] (MEH-PPV) grafted on silane-primed silicon wafer forming brushes (tether spacing d ~0.54 nm) or pancakes (d~ 7nm to 34 nm) were used to unveil the chain conformation effect as influenced by stresses on photoluminescence. Although the PL emission of all grafted single molecules red shifted with chain length, only those for the brushes followed the behavior of trapped electron with the box dimension scaled as the chain length. Upon transporting the samples betwee

Report Documentation Page

Form Approved
OMB No. 0704-0188

Public reporting burden for the collection of information is estimated to average 1 hour per response, including the time for reviewing instructions, searching existing data sources, gathering and maintaining the data needed, and completing and reviewing the collection of information. Send comments regarding this burden estimate or any other aspect of this collection of information, including suggestions for reducing this burden, to Washington Headquarters Services, Directorate for Information Operations and Reports, 1215 Jefferson Davis Highway, Suite 1204, Arlington VA 22202-4302. Respondents should be aware that notwithstanding any other provision of law, no person shall be subject to a penalty for failing to comply with a collection of information if it does not display a currently valid OMB control number.

1. REPORT DATE	2. REPORT TYPE	3. DATES COVERED
25 JUL 2012	**Final**	**11-07-2011 to 10-07-2012**

4. TITLE AND SUBTITLE	5a. CONTRACT NUMBER
Opto-Electronically Efficient Conjugated Polymers by Stress-Induced Molecular Constraints	**FA23861114055**
	5b. GRANT NUMBER
	5c. PROGRAM ELEMENT NUMBER
6. AUTHOR(S)	5d. PROJECT NUMBER
Arnold Chang-Mou Yang	5e. TASK NUMBER
	5f. WORK UNIT NUMBER
7. PERFORMING ORGANIZATION NAME(S) AND ADDRESS(ES)	8. PERFORMING ORGANIZATION REPORT NUMBER
National Tsing Hua University,101, Kuang Fu Rd, Sec 2,Hsinchu 30043,Taiwan,NA,NA	**N/A**
9. SPONSORING/MONITORING AGENCY NAME(S) AND ADDRESS(ES)	10. SPONSOR/MONITOR'S ACRONYM(S)
AOARD, UNIT 45002, APO, AP, 96338-5002	**AOARD**
	11. SPONSOR/MONITOR'S REPORT NUMBER(S)
	AOARD-114055

12. DISTRIBUTION/AVAILABILITY STATEMENT

Approved for public release; distribution unlimited

13. SUPPLEMENTARY NOTES

14. ABSTRACT

This is the final report dealing with the dramatic enhancement of optoelectronic efficiencies of conjugated polymers induced by segmental stresses discovered by the researcher, which was further studied in various fundamental facets of this important property in addition to some major breakthroughs in the road for real applications. The influences of chain conformations influenced by molecular stresses were investigated in the single-molecule systems of MEH-PPV brushes and pancakes grafted on silane-primed substrates.

15. SUBJECT TERMS

Conductive Polymers, nano photonics, Graphene

16. SECURITY CLASSIFICATION OF:			17. LIMITATION OF ABSTRACT	18. NUMBER OF PAGES	19a. NAME OF RESPONSIBLE PERSON
a. REPORT	b. ABSTRACT	c. THIS PAGE			
unclassified	**unclassified**	**unclassified**	**Same as Report (SAR)**	**48**	

n the dry state in air and wet state in the solvent, the PL spectra switched back and forth reve rsely, illustrating in the air a large blue shift up to 100 nm and the intensity enhancement. Se gmental stretching between substrate frictional points caused by coil contraction during solve nt evaporation was attributed to the observed variations arising from the state transition. For t he identical chain lengths, the segmental stretching cause by this coil retraction my produce PL enhancement up to 175 folds. Furthermore, the segmental stretching can effectively dimi nish the exciton quenching. Similar behavior was observed in the reverse way when single m olecules drop coated on the substrate was relaxed by solvent vapor imbibing.

Introduction

The energy transfer pathways following excitations from photon-absorption or electro-activation in conjugated polymers are still obscure, obstructing the optimization of the quantum efficiencies and optoelectronic applications, e.g., solar cells and light emitting diodes, of the low-cost robust materials. Thus, explorations in this area are vital for both the fundamental understanding and practical significance. In particular, the role of electron-phonon coupling generic to the soft molecular segments of conjugated polymers has been highlighted to be critical in determining the pathways. Strong electron-phonon interactions lead to the propensity of entrapment of excitons and transporting charges, facilitating heat generation or degrading chemical reactions that contribute to low quantum efficiencies and short service life.

Recently, it was demonstrated that in the conjugated polymers of MEH-PPV and P3HT multifold increases of photoluminescence (PL) efficiencies were resulted by mechanical stretching.[52-56] In addition, increases of electric conductivity (up to 5 order of magnitude) was observed when the polymer chains were confined in mesoscopic dimensions where strong residual stresses were operative. These dramatic effects were attributed to the suppression of the electron-phonon interactions in the constrained molecular states. Along a similar line, the exciton quenching commonly observed in the vicinities of the heterogenous polymer interface of a built-in voltage was switched off when the polymer chains were stretched, hinting the substantial role of electron-phonon interactions in the formation and annihilation of the excitons.

On the level of single molecules, the molecular conformations in fact reflect the status of the operative stresses. Any deviation from thermal equilibrium of the chain conformations in the final states gives rise to molecular stresses. The revelation of large effects on PL efficiencies due to variations of the chain conformations confirms the intimate connection between the energy transfer pathways and electron-phonon interactions via the molecular stresses. Furthermore, generally the molecular stress do not distribute uniformly within the single macromolecules. Therefore, molecular segments exhibit different energy transfer pathways and varied quantum efficiencies, and the distribution of which would undergo revamping when the stress was altered. For the case of single-molecules supported on substrate prepared by drop-coating, stresses are generated by the molecular stretching during the swollen-dried transition of the molecules and the anchoring points by molecule-substrate interactions separate chain segments of various stress levels. Various parameters may vary the landscape of the segmental energy transfer pathways, such as molecular weights, polymer concentrations, solvent type, and evaporation rate.

As a platform to unveil the chain conformation effect as influenced by molecular stresses, the single molecule layer of conjugated polymer MEH-PPV in the form of brushes or pancakes of different chain lengths was grafted on treated silicon substrate with the density of chain grafting varied by using graft-to or graft-from schemes. The PL spectra acquired have illustrated drastic transition between various salvation states and the transition was fully reversible. A large stress-induced enhancement effect was observed particularly for the loosely grafted pancake where the chain stretching between substrate anchoring was dominant. Separately, single molecules prepared from drop coating on silicon substrate were also investigated. Very large stress effects were observed that also manifest de-quenching of

excitons arising from the segmental chain stretching. The results acquired from these well-designed simplified molecular systems undoubted have provided important information of the stress effect on the optoelectronic behavior of conjugated polymers that shed lights onto the fundamental physics of energy transfer pathways in conjugated polymers and the viability of polymers serving as the next generation optoelectronic materials.

Experimental Section

The grafting of MEH-PPV molecular layer on silicon wafer was first proceeded by the step of cleaning and etching the silicon surface to have the Si-OH covering the substrate. It was then followed by reaction with APTMS (3-aminopropyl-trimethoxysilane) (Fig. 1a) in dilute solution. The NH_2 end-group of the APTMS molecule grafted on the silicon was then reacted with the end-group CH_2Br of the MEH-PPV monomer to start the graft-polymerization (graft-from method) or that of MEH-PPV macromolecule (graft-to) (Fig. 1a). By using the UV-Visible Absorption Spectrometer (UV-Vis), the areal density of the grafted polymer chains on APTMS was determined to be ~$3.5x10^{14}$ molecules/cm^2. The corresponding distance (*d*) between the tethered points by the graft-from method was 0.54 nm, indicating that these molecular layers were molecular brushes. The chain length of the brush was varied by changing the polymerization time. In contrast, the graft density by the graft-to methods was much lower and varied by the reaction time of the grafting processes and the size of the MEH-PPV molecules. For the molecule weights of 16k and 55k of the grafted MEH-PPV molecules, the tether spacing *d* ranging from 7 to 40 nm indicates that the grafted single molecules MEH-PPV were pancakes. The prepared single-molecule layers were analyzed by using an atomic force microscope (AFM), UV-Vis, photoluminescence spectrometer, and Fourier-Transform Infrared spectrometer (FT-IR).

In further details, prior to the APTMS grafting, the silicon surface was treated by the consecutive steps of a) acetone sonication (5 min.), b) reaction in piranha solution (H_2SO_4/H_2O_2: 2/1) for 1 hr at 120°C, and c) sonication in deionized water (5 min.) and isoproponal (5 min.), followed by HF etching in (50%, sonication), rinse in DI water (80°C 20 min. to convert the surface Si-F bonds of into Si-OH bonds), sonication in aceton (5 min.) to remove the water on the silicon surface, and then blow-dried in N_2. To graft the ATPMS, the treated silicon wafer was dipped into 1% APTMS solution in anhydrous ethanol (sonicated for 5 min. before use) for 3 min., followed by sonication cleaning in ethanol (5 min.), in ethanol/toluene (5 min.), and toluene (5 min.) to remove the non-grafted APTMS.

For the graft-from method, a monolayer of MEH-PPV monomer had to graft to the substrate first, to stabilize the surface and serve as the seeds for the subsequent graft polymerization. For this, the pretreated silicon wafer was immersed in the MEH-PPV solution (500 mg monomer in 10 ml 1:1 THF/Toluene and 0.5 ml pyridine) for 30 min. The silicon wafer was then washed in methanol and sonicated in THF. To graft-polymerize MEH-PPV on the silicon, the Monomer-g-wafer was immersed in the initiator solution (188 mg t-BuOK in 16 ml THF) with the monomer solution (250 mg MEH-PPV monomer in 30 ml THF) slowly dripped into the solution. The reaction was carried out at 60 or 70°C. The graft-polymerization may be repeated for a second time on the same wafer, usually at a higher temperature of 78°C and varied t-BuOK concentration, to increase the molecular weight. After graft-polymerization, the wafer was then sonicated in DI water to remove the t-BuOK residue on the surface, followed by additional sonication in THF for 30 min. to rid off the adsorbed MEH-PPV polymer.

For the graft-to method, MEH-PPV polymer of two different molecular weights, Mw~16k (PDI~1.05) and Mw~55k (PDI ~1.20), was first synthesized. The two polymers emitted light at 470 nm and 560 nm, respectively, in the solutions. By using the ^1H NMR (500 MHz, $CDCl_3$) spectroscopy, the chemical structures of the polymers were confirmed, and the Tolane-bis-benzyl (TBB) defects in the MEH-PPV macromolecules were determined[49,50] to be ~0.65 wt. % for the 55k g/mol. MEH-PPV and non-detectable for the

16k g/mol. polymer. From this, the average conjugation length of the higher molecular MEH-PPV was ~154 monomers while that of the lower molecular weight polymer was essentially equal to ~62 monomers. Then, solutions of two MEH-PPV polymer concentrations (2.5 mg/ml and 0.06 mg/ml) in the solvent of equal-parted THF, toluene, and cyclohexanone were prepared. The polymer was dissolved in the solvent for 24hr and then filtrated by 0.45 μm filters. The APTMS modified wafer was then reacted in the MEH-PPV solution mechanically stirred at 70°C of different reaction times for the various grafting densities. During the whole span of reaction time up to 72 hrs, no effects due to the heating at 70°C were detected on the PL properties of the to-be-grafted MEH-PPV polymer (Fig. 1e). After the grafting process, the samples were rinsed in THF, sonicated for 30min. to remove the non-grafted polymer.

Results and Discussions

APTMS primer:

As revealed by the AFM topography survey, small spots appeared as short as 30 seconds into the graft reaction, which evolved into inter-connected mild-rolling islands at 3 min. of reaction time. For longer reaction times (>6 minutes), a homogeneous film of APTMS emerged on the silicon surface. The film, however, was constructed by multiple molecular layers, as indicated by the thickness. The multi-molecular layers were joined by hydrogen bonds and hence unsuitable for chemical grafting of the MEH-PPV single molecules. Therefore, the continuous layer obtained after 3 min. was used after curing, at 130°C in vacuum oven for 3hrs, to promote the formation of Si-O-Si bonds at the APTMS-Si interface and smooth the topography as revealed by AFM (not shown). The thickness of this homogenous single APTMS layer, measured from AFM, was 0.7 nm after curing. The process of the APTMS grafting was monitored by contact angle measurements and it was found that saturation was reached after 3 min. when the contact angle plunged from ~57° to ~45°. Furthermore, in the FT-IR spectrum of APTMS modified wafer, a peak at 1114 cm^{-1} revealed the existence of the Si-O-Si bonds between APTMS and the silicon wafer, the peaks at 1597 and 3371 cm^{-1} represented the deformation and stretching signals of the NH_2 groups of the APTMS molecules, and finally the stretching of the CH_2 and CH_3 near 3000 cm^{-1}. Therefore, the APTMS were confirmed to covalently graft onto the silicon surface in the form of a uniform single molecular layer.

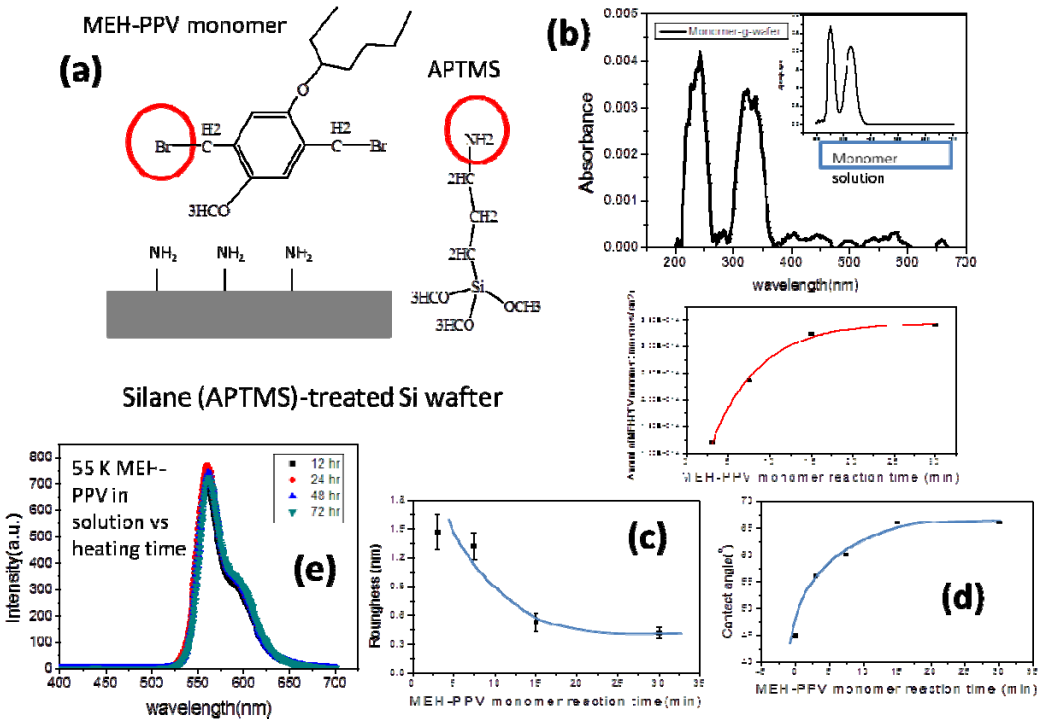

Figure 1. a) The MEH-PPV monomer, the primer APTMS, and the primed silicon surface. b) The UV-Visible spectrum of the APTMS grafted on the silicon substrate after reacting with the marker MEH-PPV monomer and the APTMS tether density as a function of the reaction time. c,d) The

roughness and the contact angle of the brushes as a function of polymerization time. e) The photoluminescence of the MEH-PPV polymer (Mw = 55k) in solution as a function of heating time at 70°C.

The density of the APTMS tethered points on silicon was estimated from the UV-Visible spectra of the APTMS-primed substrate reacted with MEH-PPV monomer. that served as the marker From the UV-Visible spectra, the amounts of grafted APTMS that reacted with MEH-PPV were calculated as a function of the APTMS grafting time, via S = A/Ɛ where S was the amount of APTMS on the substrate, A was the measured absorption from the UV-Visible spectrum, and Ɛ was the monomer absorption coefficient (1.76×10^7 mole^{-1}·cm^2) determined separately from the MEH-PPV monomer solution. It was found that the amount of graft increased with the graft time almost linearly but later saturate at around 3 min., confirming that indicated by the surface angle measurements. The saturated grafted APTMS, as given above, was 3.5×10^{14} molecules/cm^2, in good agreement with the maximum tethered silane density of 5×10^{14} molecules/cm^2 reported before.[51]

Single-Molecule Brushes by Graft-From Scheme

Since the formation of the first monomer layer grafted to the anchored APTMS was critical to the subsequent graft-polymerization for growing the brushes, the reaction of this step was examined. As unveiled by AFM, a complete layer of the grafted monomer almost formed for 7.5 min. reaction time at 60°C, and a continuous smooth layer emerged after 15 min., as revealed by the roughness (Fig. 1c). During this experiment where the initiator (t-BuOK) was absent, only one layer was formed because the monomer did not react with other. Similar trends were obtained in the surface tension by the contact angle measurements (Fig. 1d) and the grafted amount by UV-Visible spectroscopy (Fig. 1b). The saturation of the grafted monomer, as given before, was 3.5×10^{14} mole/cm^2 (Fig. 1b). The corresponding distance between the tethered points *d* was 0.54 nm. Compared to the size of the polymer to be grafted on these tethered monomer, the polymer chains only had one direction to grow during the graft polymerization, viz., normal to the substrate surface, thus forming the molecular brushes.

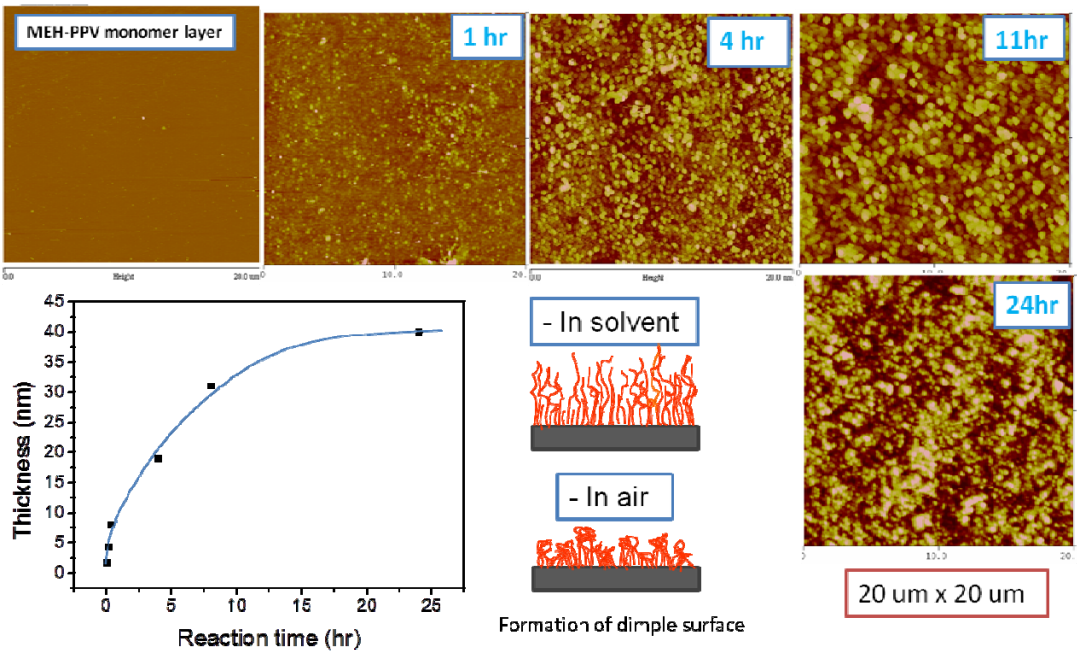

Figure 2. The AFM topography and the thickness in air of the single-molecule brushes as a function of reaction time at 60°C.

During the ensuing polymerization, small bumps protruding from the surface layer appeared and increased in size and population as the reaction time increased (Fig. 2). These bumps, upon close examination under AFM, manifested "dimpled" top surfaces that were resulted from collapse of the brushes in air. The thickness of the grafted layer increased with the reaction time, but the increase eventually slowed significantly as the monomer was being used up (Fig. 2). When the reaction temperature was raised from 60 to 70°C, the growth kinetics of the single-molecular layer remained

unchanged but the dimpled bumps increased in sizes, so did the layer thickness, indicative of accelerated chain growth at the higher temperature. To further increase the chain length of the brushes, a second-step polymerization was conducted at 70°C using a higher initiator concentration for the samples already polymerized for 12 hr at the same temperature. To estimate the molecular weight of the grafted MEH-PPV in the brushes, we calculated the average volume of one grafted MEH-PPV chain in the collapse state in air from the graft density and the layer thickness. Assuming a Gaussian statistics of the MEH-PPV molecule in the solvent state (θ state) sharing the coil volume with 19 other chains, the molecular weight was obtained by using the step length a = 0.65 nm for the MEH-PPV monomer. The molecular weight was ~63kg/mol. for 3 hr at 70°C and may reach 180kg/mol. for the samples prepared by the 2nd-step polymerization.

PL of the Single-Molecule Brushes

In the dry state in air, the fluorescence peak of the single-molecule brushes manifested a red-shifting, from 434 nm gradually to 550 nm, as the molecular weight increased from 63k to 182 k (Fig. 3a). The variation of the emission peak followed a linear dependence on the square of the brush chain length, implying the applicability of the box-trapping electron model with the chain length being scaled as the box's linear dimension and the peak frequency corresponding to the first transition level. Considering that in the spin coated films, the MEH-PPV polymers of molecular weights comparable to M_w = 63 k emit light at the peak of ~570 nm, the single molecules prepared and confined in the brushes had manifested significantly large conjugation lengths implying much less defects and chain twisting in the brush single molecules. The large peak shifts of ~130 nm between the 434 nm and ~570 nm peaks obviously was arising from the effect of inter-chain coupling on the emission although the details of the coupling remained to be explored further.

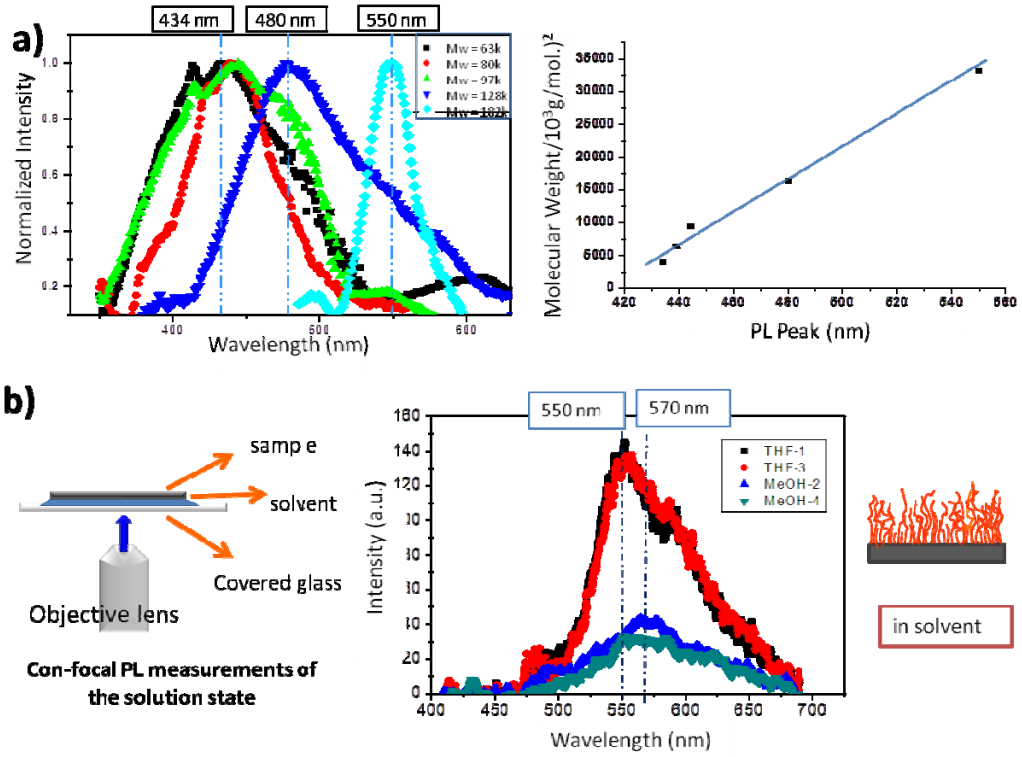

Figure 3. a) The photoluminescence spectra of the single-molecule brushes in air of various chain lengths with the intensity normalized by equal peak intensity, where a linear relationship exists for the peak emission wavelength and the square of the chain length. b) The photoluminescence of the brushes observed in the solvent environment.

For the single-molecule brushes the effect of mechanical relaxations caused by the introduction into a solution environment was studied where the photoluminescence in the solution was detected in the confocal micro-PL system with the brush sample placed face-down in a solvent bath supported on a glass slide (Fig. 3b). Confined in the brushes, the grafted single molecules manifest very small shifts,

if any, relative to that in the dry state. For example, for the longest brush chain length (182k) that was most susceptible to the transition, no peak shift was observed in the good solvent of THF although a ~20 nm red shift was detected in the bad solvent of methanol (Fig. 3b). Note that the peak shifting was fully reversible as the brushes were transporting between the good and bad solvents repeatedly. The observations indicate that the mechanical strains responsible for the dimpled topography in the dry brushes had caused only negligible effect on the peak shifting.

Single-Molecule Pancakes by Graft-To Scheme

At the early stage of the graft-to reaction, tiny bumps appeared on the substrate, each containing approximately 200-300 molecules (for the 55k MEH-PPV) or 70~100molecules (for the 16k MEH-PPV) judged from the sizes (Fig. 4). Amid the gradual increase of the bump population as the reaction progressed, partially connected structures arising from local assembly of the bumps emerged at the later stage. These aggregated structures, however, eventually gave way to the formation of the uniform surface, presumably via dissolution to the solution of the non-grafted chains. Similar behavior was observed for both more concentrated polymer concentration of 2.5mg/ml) that was near the overlap concentration c^* or that substantially lower 0.06 mg/ml.

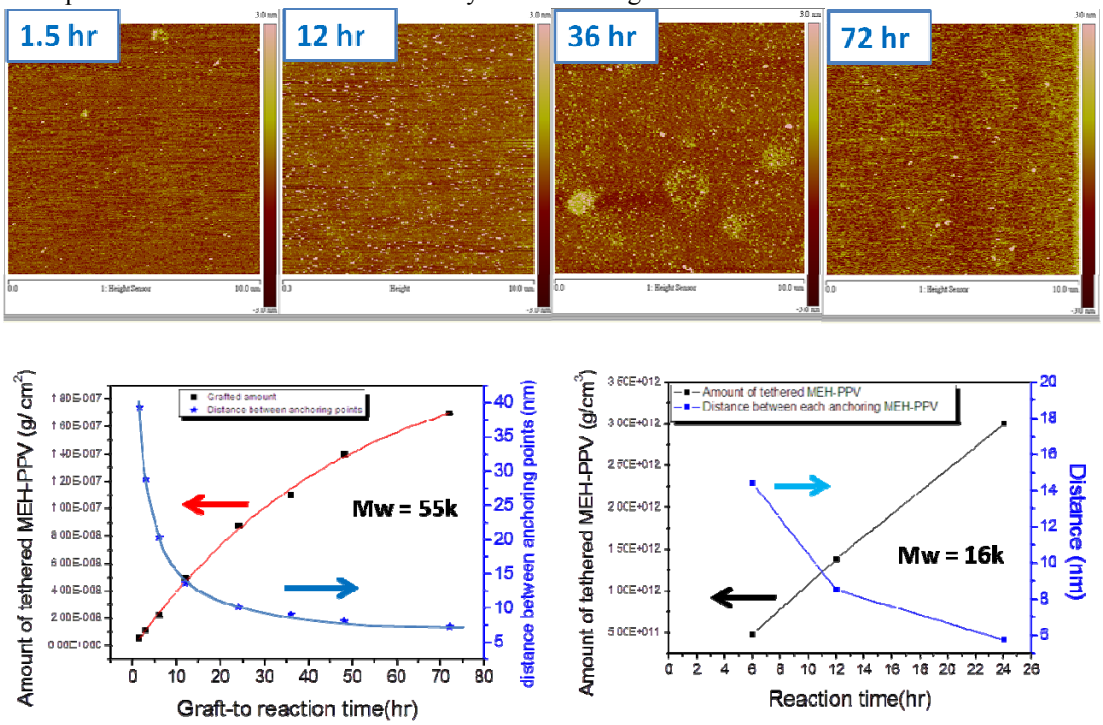

Figure 4. The process of the MEH-PPV graft-to reaction (using the polymer concentration of 2.5mg/cc) illustrated by the AFM topography of the samples (in air, Mw = 55k), the grafted amount on the substrate, and the tether spacing as a function of reaction time. .

The amounts of the graft-to polymer were determined from the samples after thorough cleaning in an ultrasonic cleaner. Careful comparisons of the AFM topography of the samples by ultrasonic cleaning and those by multiple manual solvent washes (10 times) indicated that no material losses from graft bond breakage were resulted from the ultrasonic cleaning, proving that the MEH-PPV monolayer was covalently bonded. The grafted volume was determined for the samples not yet forming the continuous layer from the bearing volumes calculated from the AFM topography, while for the one of a complete layer, it was by direct thickness measurements using AFM scanning over scratches in the film down to the silicon substrate. It was found that the grafted volume increased linearly with the reaction time but later on slowed down and saturate to a constant (Fig. 4). The rate of grafting was higher if the more dilute polymer solution (0.06 mg/ml) was used, indicating the slowing down was due to the crowding effect arising from the grafted on the substrate. Correspondingly, the spacing between the tethered points for the 55k MEH-PPV decreased from 40 nm to the saturated value of ~7nm. The tether spacing of d = 7 nm was quite comparable to the swollen size of the MEH-PPV in the solution estimated from the Gaussian model hence it was regarded to be near the smallest possible tether spacing. In fact, since polymer chains tend to spread laterally onto a flat wall,

the monolayer likely to comprise of 2D closely-packed laterally-elongated MEH-PPV molecules. Similarly, for the 16k MEH-PPV, the tether spacing d decreased from 15 nm to ~6 nm (Fig. 4).

The grafting was further confirmed by the FTIR spectra. The feature signals of MEH-PPV — the out-of-plane phenyl CH wag at 858 cm^{-1}, the alkyl-oxygen stretch at 1040 cm^{-1}, the phenyl oxygen stretching at 1204 cm^{-1}, and the semicircular phenyl stretching at 1506 cm^{-1} — were all robustly present (not shown). Conversely, the characteristic peak of APTMS at 3371 cm^{-1} diminished due to the exhaustion of NH_2 from the graft-to reactions, confirming that the MEH-PPV polymer molecules were grafted to the substrate.

Therefore, it is clear that a single layer of fully swollen MEH-PPV molecules were grafted covalently onto the substrate.

PL of the Single-Molecule Pancakes

Before grafting, the MEH-PPV emitted light in the solutions at 550 nm for the 55k MEH-PPV and 470 nm for the 16k, significantly red-shifted relative to those of the brushes (Fig. 5a). When these molecules were grafted to the substrate and dried in the air forming single-molecule pancakes, the emission peak of the 16k MEH-PPV was at 415 nm for 6 hr reaction time (d =17 nm). The peak continued to red-shift and eventually moved to 434 nm for 24 hrs reaction time (d = 6 nm) (Fig. 5a). Therefore, the 16k MEH-PPV polymers emitted light with significant blue shifts (~40 – 60 nm) relative to that in the solutions. Similarly, for the 55k MEH-PPV, the emission peak was located at 434 nm for the tether spacing of 28 nm; it was red-shifting as the tether spacing decreased, eventually to 460 nm for d = 7.3 nm (Fig. 5b). Hence, relative to the solution state, large blue shifts up to 120 nm were induced by drying in the single-molecule pancakes.

However, if immersed in the solution of toluene, the PL spectra of the grafted molecules returned to those in the solutions before grafting. This in fact was expected as the MEH-PPV molecules were grafted onto the substrate in the "stress-free" solution and hence would return to the original chain conformation state when the pancakes were immersed back in the solvent. For the 16k MEH-PPV, the emission peak was 470 nm in the wet state and would move reversible between this peak and that (550 nm) in the air when the samples were changed back and forth between these two states (Fig. 5a). The PL intensity also demonstrated a reversible enhancement when the grafted molecules were placed in the dry state. Same behavior was also observed for the higher molecular weight 55k MEH-PPV (Fig. 5b).

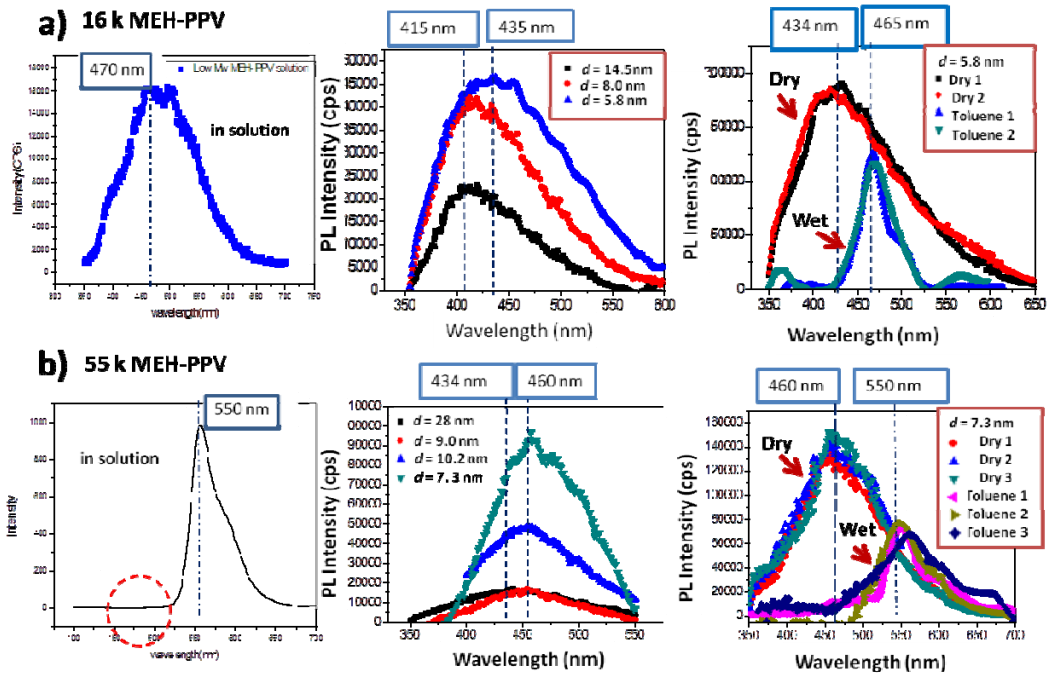

Figure 5. The photoluminescence spectra of the MEH-PPV in the solution, the grafted to the substrate with various tether spacing d's, and in the complete monolayer during the transition between the dry

state and immersion wet state, for Mw = 16k and 55k.

To unveil the cause for the blue shift in air, the pancake samples were drying slowly with the PL monitored in the confocal micro-PL system. We found that the peak did not shift at all until the stage of complete dryness. The blue shift hence was arising from the decrease of conjugation lengths when the swollen single-molecule pancakes suddenly retracted on the substrate upon rapid solvent evaporation during which chain segments were stretched between substrate friction points. This process, obviously, should be dependent on the solvent evaporation rate when the single-molecule pancakes were introduced into the air. To explore this dependence, the pancakes samples prepared by slowed solvent evaporation were examined. It was found that the emission peak in the air shifted from 460 nm to 490 nm (not shown), confirming the segmental stretching induced by rapid solvent-evaporation.

The lowering of the blue shift, relative to the emission in solution, in accompany with the decreasing *d*'s (Fig. 5) was thus reasoned to arise from declined segmental stretching forces caused by the shrinking of contact area with substrate.

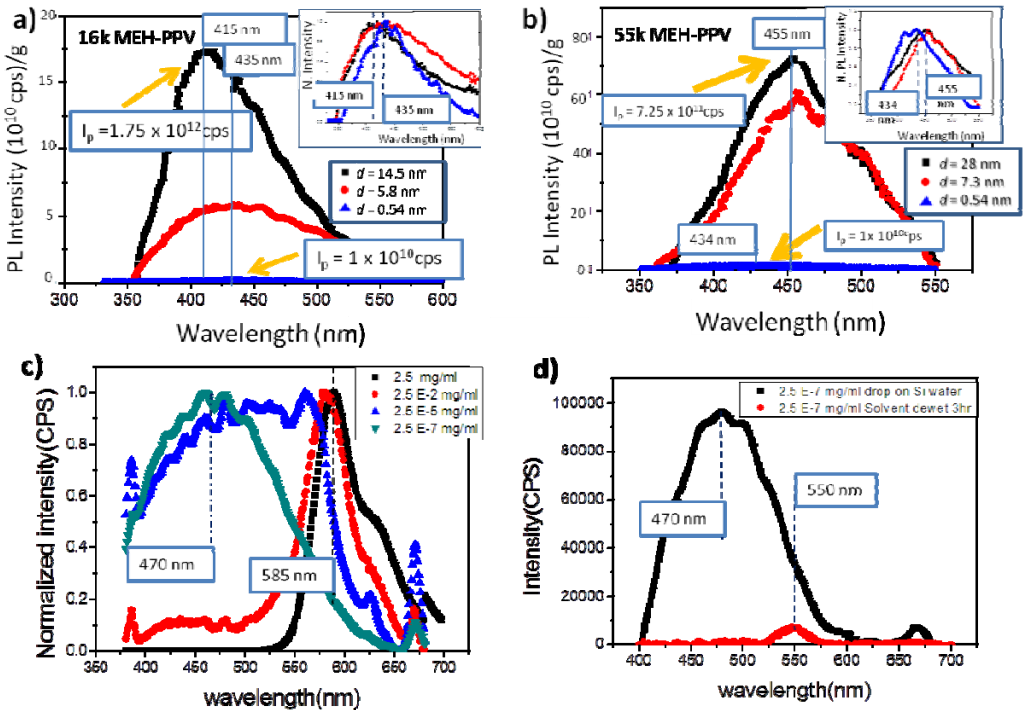

Figure 6. a,b) The PL spectra (mass-normalized) of the grafted single molecules of various tether spac ing for 16k MEH-PPV (a) and 55k MEH-PPV (b), the insets: the PL spectra illustrated with the peak i ntensity normalized to 1. c,d) The PL spectra of the drop-coated MEH-PPV for various polymer conce ntrations illustrated with the peak intensities normalized to 1. d) The variations of the PL spectra(mass -normalized) of the drop-caoted MEH-PPV (c = 2.5 x 10^{-7}mg/ml) incurred by solvent-dewetting.

PL Enhancement by Segmental Stretching

The effect of segmental stretching on the PL intensity of the grafted MEH-PPV was manifested by comparing samples of identical chain length but tethered at the various distances. To illustrate the e ffect of chain entanglements, two chain lengths, 16k MEH-PPV and 55k MEH-PPV, were used where the 16k MEH-PPV molecules, composed of only 61 monomers, were reasoned to be incapable to form chain entanglements, considering that 168 monomers are required for the soft polymer chains of poly styrene to form entanglements (M_e~17.5k g/mol.), while the 55k MEH-PPV were able, or nearly able, to undergo chain entangling. For each chain length, three values of tether spacing *d*'s were used that in cluded two pancakes samples and one brushes samples. For 16k MEH-PPV, as *d* increased from 0.54 nm (brushes samples), to 5.8 nm (pancakes samples), and to 14.5 nm (pancakes samples), the PL inten sity in air increased dramatically, from 1.0 x 10^{10} cps/g (for d = 0.54 nm) to 1.75 x 10^{12} cps/g (for d = 12.5 nm), approximately a 175-folds increase (Fig. 6a). Similar behavior was observed for 55k MEH-

PPV in that the PL intensity enhanced from 1.0 x 10^{10} cps/g for d = 0.54 nm (brushes samples) to 7.25 x 10^{11} cps/g for d = 28 nm (pancake samples), yielding an enhancement of approximately 73 folds (Fi g. 6b). Obviously, the chain segmental stretching arising from the contraction of the swollen polymer coils between friction points on the substrate may create dramatic enhancement of the PL efficiencies. For this, the chain entanglements appeared to have a tendency to lower this stretching effect, compreh ended as the chain entanglements may result portions of the molecules protected from stretching durin g the coil contraction. A smaller effect, nevertheless, was also accompanying the increase of d in that t he emission peak blue shifted with increasing d, indicating the reduction of conjugation length as a res ult of the segmental stretching.

It is important to note that a large exciton quenching field, arising from the band-alignment between MEH-PPV and the low-band-gasp silicon, was operative in spin-coated thin MEH-PPV films below 40 nm where the PL intensity when normalized to the film thickness decreased with film thickness and eventually passed through the zero point in extrapolation. Given this, the loosely grafted single-molecule pancakes used in this comparison emitted light with much stronger PL intensities although they were all below 5nm, in comparison to the densely grafted brushes of a thickness ~40 nm. Evidently, strong segmental stretching can effectively reduce this quenching effect.

Finally, a simple experiment involving drop-casting MEH-PPV molecules was conducted to further elucidate the effect of segmental stretching arising from coil contraction on a substrate. Various MEH-PPV samples (Mw = 55k) were prepared by drop-coating MEH-PPV solutions onto the unprimed pristine silicon surface with the polymer concentration c varying from c = 2.5 x 10^{-7} to 2.5 mg/ml. The PL of these samples (in air) blue shifted dramatically as the polymer concentration became very dilute, from 585 nm for the more concentrated solutions to 470 nm at c = 2.5 x 10^{-7} (Fig. 6c), indicating the remarkable fall of conjugation length as a result of segmental stretching on the substrate. When the stress gave rise to the segmental stretching was released by putting the samples in a solvent vapor environment, the peak red shift back to 550 nm with the PL intensity falling approximately 11 folds (Fig. 6d), demonstrating the dramatic effect of segmental stretching in a reverse manner.

Conclusions

The effects of segmental stretching of single-molecule MEH-PPV was illustrated by the coil contraction on grafted surface for various tether spacings and chain lengths. The segmental stretching enhanced the PL efficiencies, with the effect depending on the extent of stretching, and may go up to approximately 175 folds. In these experiments, reduction in conjugation lengths was usually observed to accompany the stretching, causing blue shift of the emission peak. Exciton quenching prevailing in the ultrathin films on the narrow-band gap substrate was switched off by the segmental stretching. Similar behavior was also observed, in a reverse way, when drop-coated single molecules were relaxed by solvent vapor imbibing.

Acknowledgments

We greatly appreciate the inspiring discussions with Günter Reiter of the University of Freiburg, Germany. We also thank the financial supports by the National Science Council of Taiwan and the US Air Force Office of Scientific Research through the Taiwan–US Air Force Nanoscience Initiative Program (AOARD-094024, -104055, and -114055).

References

1. Y. Yang and A. J. Heeger, *Applied Physics Letters*, vol. 64, 1245-1247, 1994
2. F. C. Krebs ∗, H. Spanggard, T. Kjær, M. Biancardo, J. Alstrup, *Materials Science and Engineering B*, 138 , 106–111, 2007
3. B. J. Chen, Master Thesis, Department of Materials Science and Engineering, National Tsing Hua University, 2010, Dramatic Enhancement of Optoelectronic Efficiencies of Conjugated Polymers Induced by Deweting Friction.
4. T.-Q. Nguyen,I. B. Martini,J. Liu,and B. J. Schwartz* , *J. Phys. Chem. B*, 104, 237-255 , 2000
5. K. R. Williams, Student Member, IEEE, and R. S. Muller Life Fellow, IEEE, *Journal of Microelectromechanical Systems,* vol. 5, No. 4, 1996
6. K. R. Williams, Senior Member, IEEE, K. Gupta, Student Member, IEEE, and M.

Wasilik, *Journal of Microelectromechanical Systems*, vol. 12, No. 6, 2003
7. A. V. Krasnoslobodtsev and S. N. Smirnov*, *Langmuir*, 18, 3181-3184, 2002
8. F. Zhang and M. P. Srinivasan*, *Langmuir*, 20, 2309, 2004
9. E. P. Plueddemann, Silane Coupling Agents; Plenum: New York, 1991.
10. P. F. Van Der Voort, and E. F. Vansant, *J. Liq. Chrom. & Rel. Technol.* , 19, 2718-2752, 1996
11. P. Trens, R. Denoyel, and J. Rouquerol, *Langmuir* ,11, 551-554, 1995
12. C.-H. Chiang, N.-I Liu, and J. L. Koenig, *Journal of Colloidal and Interface Science*, vol. 86, 1982.
13. S.T. Milner, *Science*, vol. 251, 1991
14. W.-C. Wu, Y. Tian, C.-Y. Chen, C.-S. Lee, Y.-J. Sheng, W.-C. Chen ,and A. K.-Y. Jen, Langmuir, 23, 2805, 2007.
15. S. J. O'shea, M.E. Welland , and T. Rayment, *Langmuir*, 9, 1826-1835, 1993
16. E. Parsonage, M. Tirrell, H. Watanabe, R. Nuzzo, *Macromol.* 20, 1361, 1987
17. H. Morschamann, M. Stamm, C. Toprakcioglu, *Macromolecules*, 24, 3681, 1991
18. I. Luzinov, D. Julthongpiput, H. Malz, J. Pionteck, and V. V. Tsukruk*, *Macromolecules*, 33, 1043, 2000.
19. V. Koutsos, E. W. van der Vegte, E. Pelletier, A. Stamouli, and G. Hadziioannou*, *Macromolecules*, 30, 4719-4726, 1997
20. D. F. Siqueira, K. Kohler, and M. Stamm, *Langmuir*, 11, 3092-3096, 1995
21. O. Prucker, and J. Ruhe, *Macromolecules*, 31, 592-601, 1998
22. M. Husseman, E. E. Malmstro1, M. McNamara, M. Mate, D.Mecerreyes, D. G. Benoit, J. L. Hedrick, P. Mansky, E. Huang, T. P. Russell, and C. J. Hawker, *Macromolecules*, 32, 1424-1431, 1999
23. R. A. Sedjo, B. K. Mirous, and W. J. Brittain, *Macromolecules*, 33, 1492-1493, 2000
24. B. Zhao and W. J. Brittain, *J. Am. Chem. Soc.*, 121, 3557-3558, 1999
25. M. Biesalski and J. Ruhe, *Macromolecules*, 32, 2309-2316 , 1999
26. E. Uchida, and Y. Ikada, *Macromolecules*, 30, 5464-5469, 1997
27. W. H. Yu, E. T. Kang, and K. G. Neoh, *J. Phys. Chem. B*, 107, 10198-10205, 2003.
28. A. Sidorenko, S. Minko, K. Schenk-Meuser, H. Duschener, and M. Stamm, *Lanmuir*, 15, 8349-8355, 1999
29. P. Paoprasert, J. W. Spalenka, D. L. Peterson, R. E. Ruther, R. J. Hamers, P. G. Evans, and P. Gopalan, *Journal of Materials Chemistry*, 20, 2651–2658, 2010.
30. S. K. Sontag, N. Marshall, and J. Locklin, *Chem. Commun.*, 3354–3356, 2009
31. N. Khanduyeva, V. Senkovskyy, T. Beryozkina, M. Horecha, M. Stamm, C. Uhrich, M. Riede, K. Leo, and A. Kiriy*, *J. Am. Chem. Soc.*, 131, 153-161, 131, 2009
32. M. Beinhoff, A. T. Appapillai, L. D. Underwood, J. E. Frommer, and K. R. Carter*, *Langmuir*, 22, 2411, 2006.
33. J. H. Moon and T. M. Swager, *Macromolecules*, 35, 6086, 2002.
34. G. Padmanaban and S. Ramakrishnan*, *J. Am. Chem. Soc.*, 122, 2244, 2000.
35. C. J. Collison,* L. J. Rothberg, V. Treemaneekarn, and Y. Li , *Macromolecules*, 34, 2346-2352, 2001
36. R. F. Cossiello, E. Kowalski, P. C. Rodrigues, L. Akcelrud, A. C. Bloise, E. R. deAzevedo, T. J. Bonagamba, and T. D. Z. Atvars*, *Macromolecules*, 38, 925, 2005.
37. P. F. barbara,* A. J. Gesquiere, S.-J. Park, and Y. J. Lee, *Acc. Chem. Res.*, 38, 602, 2005.
38. L. C. Huang, Master Thesis, Department of Materials Science and Engineering, National Tsing Hua University, 2008, Optical Harvesting Polymers in Carbon Nanotubes Network.
39. John McMurry, *Organic Chemistry*, Six Edition, Thomson
40. D. Graf, N. Grundner, and R. Schulz, *J. Vac. Sci. Technol. A,* 7, 1989.
41. T. Takahagi, A. Ishitani, and H. Kuroda, J. Appl. Phys., 69, 15, 1991.
42. L. T. Zhuravlev, *Langmuir*, 3, 316, 1987.
43. P. A. Heiney, K. Gruneberg, and J. Fang, *Langmuir*, vol. 16, 2000.

44. J. J. Pesek, I. E. Leigh, *Chemically modified surfaces*, 1993.
45. H. Okabayashi , I. Shimizu , E. Nishio, *Colloid Polym. Sci.* , 275, 744-753, 1997.
46. H.L. Chou , K.F. Lin , Y.L. Fan, and D.C. Wang, *Proceeding of the 8th Polymers for Advanced Technologies International Symposium*, 13-16, 2005
47. S.-H. Yang, C. C. Wu, C. F. Lee, and M. H. Liu, *Displays*, 29, 214–218, 2008
48. H. Becker, H. Spreitzer,* W. Kreuder, E. Kluge, H. Schenk, I. Parker, and Y. Cao, *Adv. Mater. ,* 12, No. 1, 2000.
49. H. Becker, H. Spreitzer, K. Ibrom, and W. Kreuder, *Macromol.* 32, 4925, 1999.
50. M. Atreya, S. Li, E.T. Kang, *Polymer Degradation and Stability*, 65, 287-286, 1999.
51. M. J. Wirth, H. O. Fatunmbi, in ***Chemically modified surface,*** p. 253, 1994.
52. K.-P. Tung, C.-C. Chen, P. Lee, Y.-W. Liu, T.-M. Hong, K. C. Hwang, J. H. Hsu, J. D. White, A. C.-M. Yang, *ACS Nano* **2011**, 5, 7296.
53. C. C. Chen, B. T. Chen, A. C.-M. Yang, Patents in application, Taiwan and US, 2011.
54. P. Lee, W.-C. Li, B.-J. Chen, C.-W. Yang, C.-C. Chang, Y. T. Chen, T. L. Lin, J. Tang, J.-H. Jou, et al., in submission.
55. P. Lee, *Enhancement of Photoluminescence in Conjugated Polymer Thin Film Induced by Molecular Packing Dewetting and Stretching*, Master Thesis, National Tsing Hua University, 2011.
56. P. Lee, W. C. Li, Y. Chien, G. Reiter, A. C.-M. Yang, *Photoluminescence Influenced by Chain Conformation in Thin Conjugated Polymer Films by Spin Coating and Dewetting*. American Physical Society March Meeting Dallas, TX, USA, 2011; manuscripts in preparation.

2. Ultra-Low Electric Resistivity of Conjugated Polymers Confined in Mesoscopic Thin Films

Electric resistivity of conjugated polymer poly(3-hexylthiophene) (P3HT) confined in ultrathin films was found to decrease significantly, plunging ~5 orders to ~7 x 10^2 -cm at thickness (.)~2 nm, in spin coated films and thin grafts on carbon nanotubes. The decrease of electric resistivity appeared to be less sensitive to conformation-coordinated chain ordering, if any, but more on the degree of mechanical constraint restricting the molecular segmental mobility. The resistivity decreased exponentially with film thickness but illustrated a transition at ~100 nm below which the residual stress increased and the resistivity decrease became much more significant. The behavior was consistent with the Mott's hopping model that unveiled a sharp reduction of charge localization radius, from 5 nm to 0.5 nm, in the ultrathin films, accompanied by a proportionally increased density of states. This effect is attributed to the drastic reduction of charge trapping arising from the suppression of electron-phonon interactions in the constrained polymer chains confined in mesoscopic dimensions.

Introduction

The underlying physics of charge transport in conjugated polymers[1-28] is still obscure in the molecular details,[11-25,29-31] and this deficiency is echoed by the charge transport-related bottlenecks of the development of polymer-based microelectronics, e.g., low optoelectronic efficiencies, short service life, and inferior conductivity.[1,4-8,24] Therefore, unveiling the physics of charge transport in mesoscopic polymers is pivotal for the development of the polymer-based devices such as solar cells, light emitting diodes, and thin film transistors. One unique property of the long chain-like molecules of polymers is the inherently flexible backbone molecular architectures that vary local segmental lengths by facile rotations of the joining monomers. Therefore, upon introduction of a perturbing Coulomb field stemming from excitation of the electronic states, segmental thermal vibrations of the polymer molecules that are generally packed in disorder in thin solid films readily relax the

perturbations and result local molecular deformations around the excited states. The effective mass of the charge thus increases, thereby likely leading to self-trapping of the excited states[3-8] to give rise to low radiative efficiencies and short service life. The time scales of this electron-phonon coupling are believably within 100 – 300 fs. When the coupling is suppressed, enhancements of the optoelectronic efficiencies, for example, are expected to arise. Recently, tensile stretching was shown to produce large enhancements of the optoelectronic efficiencies and life of conjugated polymers,[35-39] a good illustration for what could happen when the coupling were suppressed in the stress-rigidified chains.

Further to electro-excitation, the transport of the excited states (charge transport) was often treated as being conducted via incoherent hopping among localized sites (states). The hopping was allegedly influenced by the way how chromophores communicate with each other via the long-range Coulomb interactions as well as the coupling of nuclear motions of the field-inflicted chains and the surrounding.[34] In contrast, coherent charge transport on the extended scales was observed when the electron-phonon interactions were fully suppressed, as in the case of polyacetylene confined in the monomer crystal.[32] As a simplification for portraying the mechanistic aspects of charge transport, the hopping model originally devised by Mott[1,40-44] for amorphous inorganic semiconductors was often borrowed for polymers despite the fundamental difference in the *k-E* structure.[18-22] A distinguished feature of the hopping model is the exponential decrease of the electric conductivity with decreasing film thickness. Although this characteristic behavior has long been observed in inorganic amorphous semiconductors,[40-44] no such conclusion has yet arrived for polymers.[26-28]

As an attempt to clarify this controversy, we underwent exploration on the charge transport in mesoscopic polymers. First of all, from literature, the charge mobility in polymers was theoretically predicted, based on the transport bandwidths under the condition of no charge trapping or scattering, to be in the order of 10^3 cm^2/Vs, many orders higher than the bulk.[4] By the same token, electric conductivity was alleged to increase dramatically for the transport distances too short for charge trapping or scattering to occur.[4,24] The theoretical assertion was later empirically supported by the high-frequency measurements (charge mobility ~30 cm^2/V-s at ~30 GHz)[7] and the low effective electron masses in relaxation-free polymers (~0.05 m_e).[5,8] Others supporting evidence includes the orientation-dependent high mobility of ~0.1 cm^2/Vs in P3HT thin films of field-effect transistors (FETs),[11-15] and the superb mobility that reached a few cm^2/Vs in the substrate-interacting 2D-spatially-correlated ultrathin layers in FET.[13,16,17] All these had clearly indicated that charge transport in mesoscopic polymers may be enhanced orders of magnitude relative to the bulk due to the absence of charge trapping, chain ordering, or special interactions with the adhering substrate. However, the molecular constraint effect prevailing in the mesoscopic polymers, particularly that by the residual stresses, which may be directly connected to parts of these observations, has never been explored. It is well known that polymer molecules when confined in mesoscopic dimensions are constrained by substantial stresses arising from the highly distorted chain conformations.[46-48] A large effect is thus expected to emerge on charge transport in these systems where the electron-phonon coupling is suppressed.

Therefore, in this work, charge transport in the conjugated polymer poly(3-hexylthiophene) (P3HT) of mesoscopic dimensions was determined and studied in the light of the stress effects. Two entirely different approaches were employed for the experiments. In addition to the spin coated thin films that are widely used, thin P3HT layers grafted on carbon nanotubes (CNTs)[49-55] were also prepared and investigated.[50,56-58] The results clearly reveal a charge transport mechanism describable by charge hopping that is highly sensitive to molecular stresses. The implications of the unveiled physics may be useful for the microelectronic applications based on polymers.

Experimental Section`

Raw Materials

Multi-walled CNTs (purity ~ 95 %, conductivity > 10^{-2} S/cm) were purchased from

the Applied Nanotechnologies Inc. The outer radius of the CNT was measured under TEM to be ~12nm. The graft agent 2-(3-thienylethanol) (3TE) (99%) and the 3HT monomer (98%) were purchased from Acros Organics. Polystyrene (PS), the matrix polymer for the P3HT-grafted CNTs, was acquired from the Pressure Chemical Company (Mw = 2,000,000g/mol., PDI= 1.06). All were used without further purification.

Grafting P3HT on CNTs

Detailed descriptions of the steps for grafting P3HT on CNTs of controlled thicknesses were reported elsewhere[49,51] and these are hence described briefly here. Firstly, chain grafting sites of carboxyl groups, with an average spacing of ~0.9 nm, were created on CNTs by acid treatments,[50] after which the average CNT length was reduced to ~2 m. Upon washing in deionized water, the CNTs were dried and then reacted with thionyl chloride ($SOCl_2$), 3TE, pyridine, and DMAC at 90˚C to anchor 3TE on the CNTs (Scheme 1).[59] Short P3HT chains were then grown to ~2nm thick from the anchored 3TE groups via continuous reactions with the 3HT monomer catalyzed under $FeCl_3$ at 2˚C in acetonitrile. The collected product at this step was termed CNT-P-2. The chain length of the anchored P3HT may be increased by further reactions with 3HT monomer in chloroform at 2˚C catalyzed under $FeCl_3$. The chain length and thus the graft thickness were controlled by the length of reaction time, the catalyst concentration, and the solvent blend composition. In this manner, two additional graft thicknesses were prepared: 4 nm (CNT-P-4) and 8 nm (CNT-P-8). No thicker grafts were prepared because P3HT crosslinking that could lead to CNT aggregation emerged for thicknesses greater than ~15 nm.[51] The thicknesses of the P3HT grafting were measured under a transmission electron microscope (TEM, JEOL JEM-2010) and checked by weight losses obtained from the thermogravimetric scans (TGA, Perkin-Elmer).[49-55]

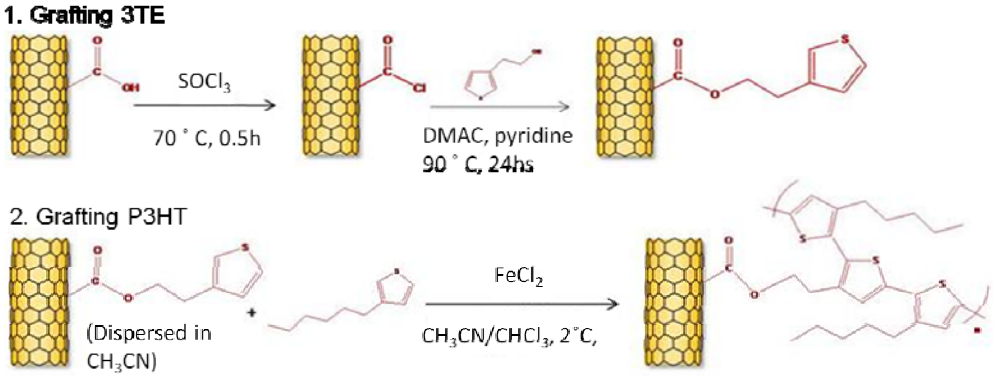

Scheme 1. Grafting P3HT on CNTs

The molecular weights (MW) of these grafted P3HT molecules were determined by using gel permeation chromatography (GPC) after having scissor the whole grafted P3HT from CNTs using KOH reflux,[50,52,53] to be 13kg/mol. (CNT-P-2), 30kg/mol. (CNT-P-4), and 66kg/mol. (CNT-P-8).[51] The regioregularity of the P3HT, determined by comparing the signals at chemical shifts of ca. 2.80 [head-to-tail] and 2.58 [head-to-head] ppm in the ^1H NMR spectra,[60] was ~80%.[51] The neat resin of P3HT (MW= 66kg/mol., regioregularity~80%) was also prepared following the similar scheme for the use in the experiments. Detailed reaction results are summarized in Table 1 in the Supplemental section.

Resistivity Measurements

For resistivity measurements, where a Keithley 2400 source meter was used, samples around 25 m of CNTs-P3HT dispersed in PS were prepared by drop coating on ITO glass from the solutions. In addition, thin films of neat resins of P3HT and PS with thicknesses in the range

from 5 nm to 2000 nm were prepared by spin coating on ITO glass slides. Before use, the films were examined under both the optical microscope and atomic force microscope (Veeco, Dimension™ 3100) to screen the ones containing defects or pinholes. In order to remove the CNT orientation effect, the conductivity of the thick film samples of grafted CNT in PS was measured in both the horizontal (in-plane) and vertical (through-thickness) directions. The horizontal resistance was measured by using a 4-point probe method on the top of the samples (electrode spacing ~1000 μm). The vertical direction was determined from sandwiched samples of ITO-polymer film-ITO as a function of compressive force ensuring good electric contact until stable readings were obtained (Fig. 1a). For the samples of grafted CNT in the PS matrix, no effects of the "skin layer" on the measurements were detected, as revealed by comparing etched samples of which the top layer of ~60 nm was removed by oxygen plasma (60 W, 10 minutes) (Fig. S1 of Supplemental). For the spin coated films, the resistance measured manifested a time-dependent behavior (Fig. 1b), and the data was taken after a contact time of ~300 second when they became saturate.

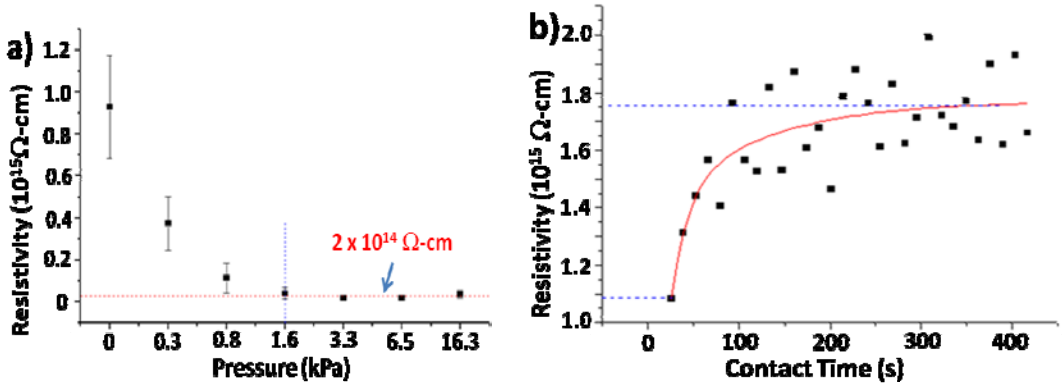

Figure 1. a) Resistivity measurements vs. sandwich pressure (data: 100 nm spin-coated PS films), and b) resistivity measurements vs. contact time during the electric tests. (data: 500 nm spin-coated PS films).

Results and Discussions

Resistivity of P3HT on CNTs

Under TEM, the thicknesses measured from the P3HT coatings wrapping around each CNTs in a smooth and conformal manner (Fig. 2a-c) were in good agreement with those obtained from the TGA scans— CNT-P-2: 2.1±0.6 nm (TEM), 2.7 nm (TGA); CNT-P-4: 3.6±1.1 nm (TEM), 3.5 nm (TGA); CNT-P-8: 8.3±1.3 nm (TEM), 7.9 nm (TGA).[51] The number of grafted chains per unit area— 0.11 chains nm^{-2} (CNT-P-2), 0.08 chains nm^{-2} (CNT-P-4), and 0.10 chains nm^{-2} (CNT-P-8), calculated from the MW and thickness (assuming a constant mass density ~1g/cc for the coating),[51] manifested only weak dependence on the thickness, indicating that the graft layers thickened due dominantly to the growth of the P3HT chain anchored at the beginning. The spacing between grafted chains was calculated to be ranging from 3.0 to 3.5 nm, significantly smaller than the radii of gyration of the macromolecules, indicating that the polymer molecules were constrained in the brush-like packing far deviating from the thermal equilibrium conformations.[49-51]

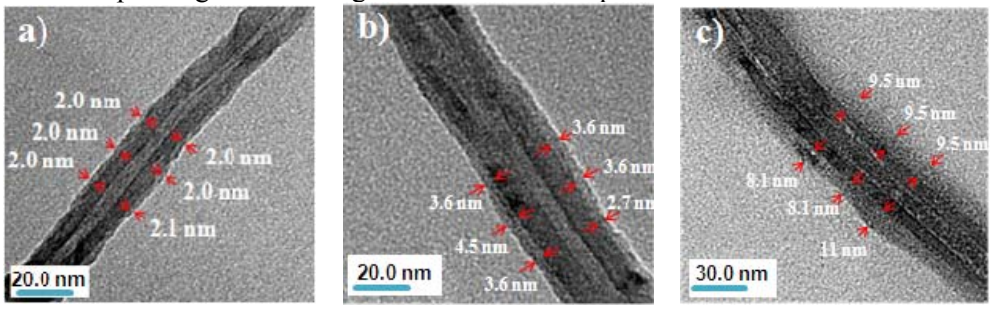

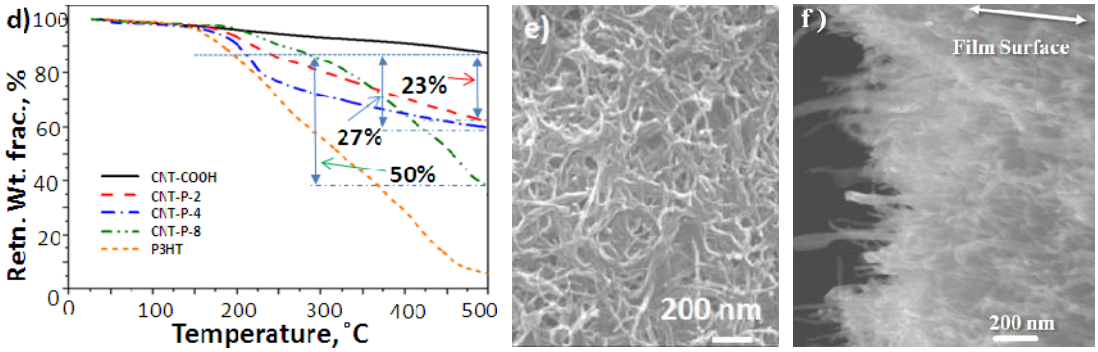

Figure 2. a-c) TEM micrographs of the P3HT-grafted CNTs: a) CNT-P-2, b) CNT-P-4, c) CNT-P-8; d) TGA curves of the acid-treated CNT (CNT-COOH), CNT-P-2, CNT-P-4, CNT-P-8 and P3HT with a heating rate of 10˚C / min under argon. e) SEM micrograph on the surface of the nanocomposite film (ϕ = 90 wt.%). f) SEM micrograph of a cross-section edge of freeze-fractured films (ϕ = 90 wt.%) illustrating strongly CNT orientation parallel to film surface.

The P3HT-coated CNTs dispersed uniformly into the PS,[49-55] forming a percolated CNT-network for electron transport. With the CNTs orienting strongly to the film surface (Figs. 2e, 2f), the nanocomposites manifested anisotropic conduction with resistivity in the vertical direction (ρ_v) approximately 3 orders higher than that in the horizontal direction (ρ_h). Therefore, charge conduction was analyzed in both the horizontal and vertical directions using the percolation scaling law $\rho = \rho_0(\phi - \phi_c)^{-t}$ in order to extract the resistivity of the thin P3HT coating, where ρ and ρ_0 were resistivity of the nanocomposite and the P3HT-grafted CNTs, ϕ_c was the percolation threshold, and t was the conductivity exponent (Fig. 3a).[56-58] As revealed by the percolation analyses (Table 2, Supplemental), the electric conductance of the nanocomposite was found to follow the percolation behavior in both directions with the percolation threshold ϕ_c determined to be ~0.001 – 0.003 wt.% in the horizontal direction, about 3-4 orders lower than that in the vertical direction (~9.0 wt.%). This indicates the much more effective percolation in the horizontal direction as compared to that in the vertical direction, consistent with the observed preferred CNT orientation. Arising from efficient percolation that requiring much a smaller number of CNT contacts that dominated the resistance in the percolation pathways,[61] the resistivity ρ_0 in the horizontal direction ($\rho_{0,h}$) was about 1000 folds lower than the vertical ($\rho_{0,v}$). This anisotropy was observed to be of the similar degree for all graft thicknesses, including the bare CNTs, as illustrated by the almost parallel curves of resistivity vs. graft thickness (Fig. 3b). It is important to note that, given the large variations in the percolation structures, the consistent percolation behavior of the conductance along these two directions clearly indicates negligible contributions from local irregularities, e.g., CNT shorting, consistent with the robust P3HT coatings on CNTs.

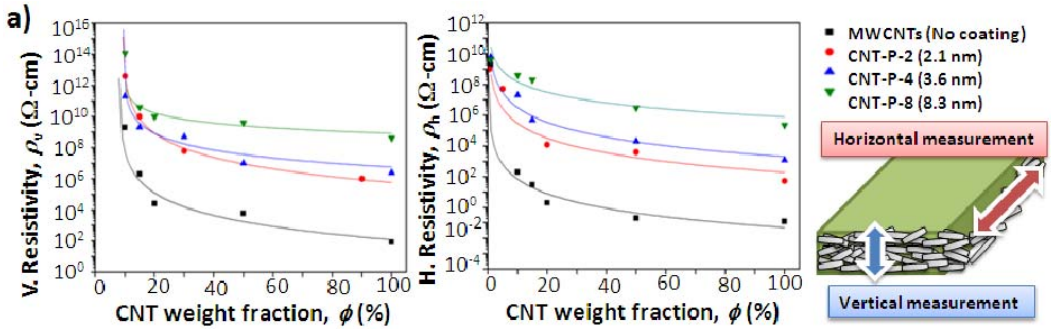

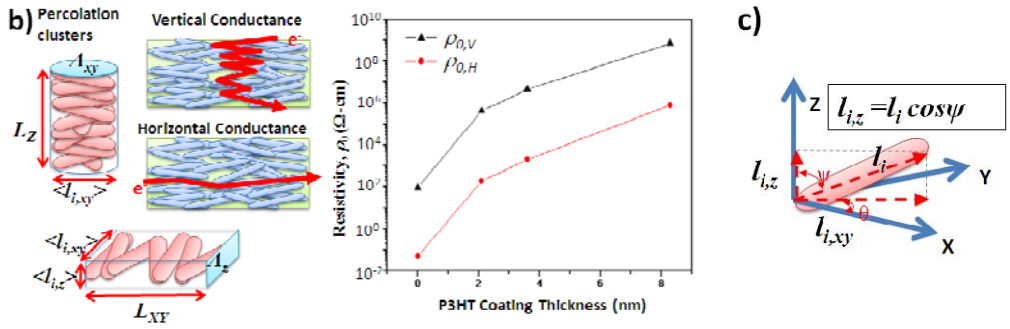

Figure 3. a) The vertical and horizontal resistivity of the nanocomposite films vs. . b) Schematic depictions of the percolation clusters for the vertical and horizontal conductance in CNT-PS nanocomposites, and the derived resistivity of both the percolation directions as a function of the P3HT coating thickness. c) Definitions of the inclination angle ( ) and azimuthal angle ( ) of the CNT rod of length l_i in a coordinates system where the *Z*-axis is parallel to the film thickness.

The resistivity of the thin P3HT coatings on CNTs was obtained once the numbers of CNT contacts were determined. For this, the CNT orientation in the nanocomposites was analyzed using the similar approach to that for dipoles alignment. By this, each CNT was assumed to orient in the nanocomposite following a Boltzmann distribution under the potential energy $E_i(\varphi) = -F_{xy} l_i |cos(90°-\varphi)|$ arising from the alignment force F where l_i was the CNT length, φ was the CNT tilt angle with the Z axis parallel to the vertical direction (Fig. 3c). For each direction, the conductance percolation was assumed to follow the shortest pathway that requires the least possible CNT contact points (Fig. 3b) inasmuch that the statistically expected numbers of CNT contacts in the vertical and horizontal conductance, n_v and n_h, were simply $n_v = L_z / \langle l_{i,z} \rangle$ and $n_h = L_{xy} / \langle l_{i,xy} \rangle$ where L_z and L_{xy} were the thickness and length of the nanocomposite samples, and $<l_{i,z}>$ and $<l_{i,xy}>$ were the average CNT projected lengths in the vertical and horizontal directions readily evaluated once the force F was given. Furthermore, the contact resistance (R_c) between the two joining CNTs was related to the nanocomposite resistivity $_0$ obtained from the percolation analyses $n_v R_c = \rho_{0,v} \frac{L_z}{(< l_{i,xy} > / 2)^2 \pi}$ or $n_h R_c = \rho_{0,h} \frac{L_{xy}}{\langle l_{i,xy} \rangle \langle l_{i,z} \rangle}$. Applying the condition that R_c obtained for either directions should be identical, the force F and R_c were determined. The force F, arising from CNT self-organization driven by solvent evaporation during sample preparation, was found to be ~ $-50 k_B T / l_i$, approximately constant for all systems explored here. The contact resistance R_c for the un-coated CNTs was determined to be $1.2 \times 10^4 \Omega$, on the same order as that reported for single-walled CNTs.[62] For the P3HT-grafted CNTs, the obtained R_c was used to calculate the resistivity of the thin grafted P3HT via $R_c = \rho_{P3HT}$ (2 $/A_c$) where τ was the graft thickness and A_c the contact area of CNTs approximated as the square of the CNTs' diameter (Table 3, of the Supplemental).[50] The resistivity ρ_{P3HT} was found to be several orders lower than the bulk (~$10^7 - 10^8$ Ω-cm),[9-10] equal to 1.1 x 10^6 Ω -cm for τ = 8.3 nm, 5.5 x 10^3 Ω -cm for τ = 3.6 nm, and 7.0 x 10^2 Ω -cm for τ = 2.1 nm, decreasing rapidly with reducing coating thickness (Fig. 4a).

Resistivity of Spin-Coated Films

The resistivity of the spin coated film clamped between two ITO electrodes was then determined, from = 5 nm to 2000 nm, for comparison with those grafted on CNTs. The obtained resistivity of the spin-coated P3HT films with greater than 100 nm was very close to that reported for bulk P3HT. The resistivity then decreased rapidly with reducing for films thinner than =100 nm, plunging to ~10^4 -cm at = 5 nm (Fig. 4a),

comparable to those obtained from the thin P3HT grafted on CNTs. It is important to note that these macromolecules packed in the spin coated thin films was of the pancake-like molecular conformations laterally elongated parallel to the film to give rise to the large equi-biaxial residual stresses.[46,47] This type of conformations was very different from that in the brush-like packing of the thin grafts on CNTs. Thus, the chain orderings in these two systems, if any, were quite different. Nevertheless, these two systems shared the similarity of large deviations from thermal equilibrium, indicative of significant confinement stresses imposed on the chain segments.

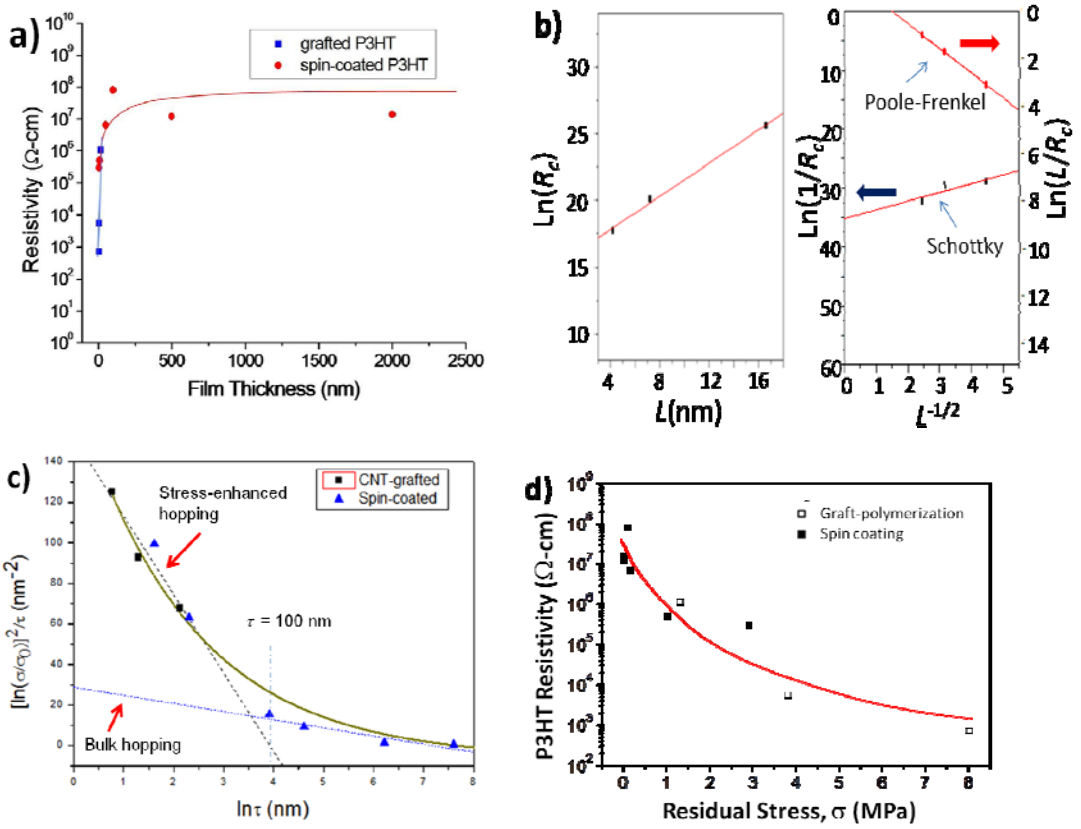

Figure 4. a) The resistivity of the grafted P3HT derived from the contact resistance from the nanocomposites vs. the grafting thickness. b) The single-event electron tunneling was examined by plotting $ln(R_c)$ vs. L to obtain the value of k; the effects of current leakage were analyzed by plotting ln $(1/R_c)$ (Schottky emissions) or $ln(L/R_c)$ (Poole-Frenkel emission) versus $L^{1/2}$. c) The resistivity of spin coating PS films versus the film thickness. d) The resistivity of spin-coated P3HT film and grafted P3HT vs. residual stress.

Single-Event Tunneling and Leakage Currents

The plunge of the electric resistivity in the low thickness regime was further analyzed to detect the influences arising from the single-event tunneling and leak currents between the electrodes.[63] For the single-event tunneling, the current between the CNTs separated by an energy barrier of $_0$ was given by $I = c\rho_A\rho_B \bullet \exp(-Lk)$, where ρ_A and ρ_B were the densities of states in the two contacting CNTs, L was the distance between the CNTs, the parameter k defined as $k \equiv \sqrt{2m_e(\Phi_0 - E)/\hbar^2}$ contained the activation energy of E resulted by the applied voltage V, and c was a system constant.[6-8] Therefore, the contact resistance between the CNTs was given as

$$R_c = \frac{V}{I} = \frac{V_i}{c\rho_A\rho_B e^{-Lk}} = ae^{Lk}$$

where *a* is the constant. Therefore, in a plot of $ln(R_c)$ vs. *L*, the data followed a straight line from which the value of *k* was obtained from the slope, to be 0.62 (Fig. 4b). Since the work function of CNT was 5.2 eV and the lowest unoccupied molecular orbital (LUMO) of P3HT is 3.2 eV, $_0$ was ~2.0 eV. Using the determined value for *k*, the activation energy *E* would be ~ 1.93 eV, indicating that the applied voltage *V* at the contact point needed to be 1.93 V for producing the measured current. However, since the actual voltage between contacting CNTs was only ~0.1 mV, about 4 orders lower than that required for the single-event tunneling, the contribution from this source was negligible.

Next, the effect of the leakage current *I* was examined. The leakage current between electrodes is described as $I \propto \exp(\Gamma)$ for the Schottky emissions or $I \propto \frac{\exp(\Gamma)}{L}$ for the Poole-Frenkel emissions,[63] where $\Gamma \equiv \left[\left(-q\Phi_0 + q\sqrt{qV/4\pi L\varepsilon_0\varepsilon_r}\right)/k_BT\right]$ in which *q* was the charge, and ε_0 and ε_r were the permittivities of vacuum (8.85×10^{-12} A·s/V·m) and P3HT, respectively. The resistivity data were found to follow straight lines in the plots of $ln(1/R_c)$ vs. $L^{-1/2}$ (Schottky) and $ln(\ /R_c)$ vs. $L^{-1/2}$ (Poole-Frenkel), only that the values obtained for $V/\ _r$ from the slopes were both unreasonably large (Fig. 4b). With the dielectric constant ε_r of P3HT to be 6.5,[64] the values of *V* determined for the Schottky emissions was 54.5 V and Poole-Frenkel emission to be 82.6 V, both too high compared to the actual applied voltage of ~0.1mV.

In short, these contributions from the Schottky emissions, the Poole-Frenkel emissions, and the single-event tunneling between electrodes to the conductivity measurements were insignificant and could be ignored.

Charge Hopping

The steep changes of the resistivity with thickness were found to follow the general exponential dependence. In fact, the exponential dependence implies that the conduction mechanisms operative in the polymer systems were based on strings of independent events, such as hopping, by charges. Hopping of charges, as a conduction mechanism in polymers, is extended from that proposed for semiconductors and glasses, by Miller and Abrahams, Mott, and Pollack and Hauser,[41-45] where the conductivity is assumed to be dominated by electron hopping described as[1,42]

$$\sigma \propto \exp\left[-(T_0/T)^{1/4}\right],\ T_0 = \beta/ga^3,$$

where *g* is the density of localized state, *a* is the electron wavefunction localization radius, and is a numerical factor containing the thickness dependence.[1] Essentially, the charge hops (or tunnels) under the influence of the applied electric field, between small "local spots" of high polarization that provide local charge levels, over energy barriers of the order of $\sim e^2/\ _rR$ where $_r$ is the local dielectric constant and *R* is the distance between the local spots, forming a pathway connecting the film surfaces.[42] These pathways, in fact, may be viewed as "punctures" of the insulator, and for polymers the conductivity may be expressed as[1,21, 65,66]

$$\sigma = \sigma_0 \exp(-2\sqrt{\frac{2\tau\lambda_T}{a}})$$

where σ_0 is the conductivity prefactor (for P3HT, $\sigma_0 = 1.6\times10^4$ S/cm),[23] λ_T is defined as $\lambda_T = ln\ \lambda_T - ln(gkTa\tau^2) \approx -ln(gkTa\tau^2)$. Rearranged, σ is expressed as[1,21]

$$\frac{[\ln(\sigma/\sigma_0)]^2}{\tau} \approx -\frac{16}{a}\ln\tau - \frac{8}{a}\ln(g_0kTa).$$

Hence, the parameters *a* and *g* characteristic of the charge hopping are acquired from the resistivity data from the plot of $[\ln(\sigma/\sigma_0)]^2/\tau$ versus $\ln\tau$.

The resistivity data, when plotted in $[\ln(\sigma/\sigma_0)]^2/\tau$ versus $\ln\tau$ (Fig. 4c), elucidated

a transition at $\tau \sim 100$ nm with varied exponential dependence in the thickness regimes above and below. It indicated that charge hopping may be used to describe the charge transport in the polymer, and that the hopping underwent dramatic modifications as the polymer chains were packed into small geometries below the molecular dimensions of the giant molecules. It was further found that in the regime below 100 nm, we obtained a = 0.45 nm and g = 1.0 x 10^{17} $J^{-1}nm^{-3}$, although a subtle trend of changes indicative of progressively decreasing a and increasing g for even smaller thicknesses were noted. This result is comparable to that obtained from mobility measurements on the TFT devices, a = 0.6 nm, where the thicknesses fell into the same category.[23,25] Conversely, for the thicker films (τ > 100 nm), a = 5.4 nm and g = 1.8 x 10^{13} $J^{-1}nm^{-3}$ were obtained, for which the magnitude of a was consistent with the expected length scales for ordinary charge relaxation in polymer as implied by the exciton geometry relaxation of 2.0 - 2.5 nm.[33] Evidently, as polymer molecules are confined in films below 100 nm, the localization radius decreased substantially in company with the increase of density of state g to give rise to the dramatic growth of electric conductivity. Across the sharp transition at $\tau \sim 100$ nm, however, the total number of allowed localized states, $\sim a^3 g$, changed only modestly to be within the same order of magnitude, implying that the dramatic increase of the electric conductivity mainly arose from the mechanistic changes of the hopping, rather than variations of the available charge densities.

Polymer Confined in Small Dimensions

It is well known that polymer chains in ultrathin films are subject to large residual stresses originated from significant deviations from their thermal equilibrium conformations.[45-48] Constrained under these stresses, the polymer chains are restricted in segmental motions to the extents dependent on the stress magnitude and local packing. Since charge relaxation requires local molecular deformations,[3,42] which basically are time integrations of biased molecular vibrations, charge trapping is suppressed in these molecular chains, leading to decreased effective carrier masses and the rapid increase of electric conductivity. Reasonable correlation was obtained between the electric resistivity of P3HT and the residual stresses estimated from the measurements of PS films of similar thicknesses(Fig. 4d).[46,48] In addition, despite that the chain confinement states varied in the grafted and spin coated P3HTs, the deviations from the thermal equilibrium in both cases were large enough such that the differences in the residual stresses and thus the resistivity were insignificant in comparison to that due to chain confinement.

Although further experiments are clearly in need, we may postulate a simple model to account for the charge hopping behavior observed here. Obviously, since polymer solids are assemblies of chains packed in disorder, local heterogeneities prevail arising from packing fluctuations and lead to "local sites" of polarizations of various extents positively or negatively deviated from the average under the external field. Driven by the Coulomb interactions and thermal activation, electron tunneling occurs from one site to another, giving rise to charge hopping and long distance transport. These charged centers retain charges for various periods of time conditional on the degree of chain relaxation from the electron-phonon interactions during the dynamic transport processes. Following Mott[42], the activation barrier due to the electron-phonon interactions over which the charge has to overcome to hop out the site is $V(r) = -\frac{q^2}{2r}\left(\frac{1}{k_\infty} - \frac{1}{k_0}\right)$ where q is the local charge, k_∞ and k_0 are respectively the high frequency and static dielectric constants. In addition, the hopping frequency is proportional to $C \cdot \exp(-aR) \cdot \exp(-V/kT)$ where R is the hopping distance and C is a constant. Furthermore, the activation energy is essentially the polaron energy $\sim \frac{1}{2}\sum \alpha_{ep} \hbar \Omega_p$ where Ω_p is the angular frequency for an optical mode of the wavenumber p and α_{ep} is the electron-phonon coupling constant for that optical mode. As the

electron-phonon interactions reduced in the stress-constrained polymer chains confined in ultrathin films, α_{ep} decreased, so did the trapping, leading to increases of the jump frequency. Moreover, information regarding R as influenced by the confinement may be explored from further analysis of the conduction pathways, e.g., the linear resistance networks,[40] but even without it, the jump frequency is predicted to increase as the localization radius a decreases, consistent with the behavior of electric conductivity in the confined states. Thus, the simple model proposed by Mott seems to provide a useful guide to understand charge hopping in polymers. It is meaningful to point out that, electron-phonon interactions may help reduce the tunneling barrier heights to facilitate charge transport in the limit of small thermal coupling.[67] However, in the strong coupling regime such as the polymers explored here, the dynamics interactions between chain vibration and charge transport have never been rigorously explored. As clearly elucidated this work, constraining the segmental motions of polymer chains significantly boosts electric transport. Thus, the mechanical properties on the molecular scales, either elastic or plastic flows, are very important for properly understanding the electron-phonon interactions and their effects on the optoelectronic and electronic behavior in the polymer glasses.

The effect of stresses via electron-phonon interactions may also be used to explain the ultrafast behavior of ~100 fs. Since in the ultrafast regime the time scales are below the threshold of transition from the in-phase transportation to the incoherent hopping,[3,33,34] the electric transport is likely to be free from charge trapping and thus manifests very efficient transport. Finally, the ultralow resistivity obtained for the 2 nm P3HT here, in fact, corresponds to the charge mobility of ~ $3cm^2/Vs$ if a carrier density of ~10^{-2} Cm^{-3} determined under the flat-band condition[24] was used. This, however, is still significantly lower than the ultrafast measurements of ~30 $cm^2/V\text{-}s$ or the theoretical predictions in the order of 10^3 cm^2 $V^{-1}s^{-1}$ based on the bandwidth of ~1 eVs.[4] It thus implies that even lower resistivity may be obtained for P3HT in the further constrained states.

Conclusions

A striking effect on the electric resistivity of conjugated polymer films was observed when the film thickness is reduced to the regime where the giant molecules are confined such that the electron-phonon interactions are effectively suppressed. The electric resistivity decreased approximately 5 orders of magnitude when the film thickness was reduced to ~2nm. This effect was observed in the confining systems of varied molecular conformations, hence strongly indicating that molecular ordering played a lesser role relative to the propensity to form charge-trapping local deformations. The Mott's charge hopping model can be used as a framework to describe the mechanistic features of the observations, revealing that the decrease of electric resistivity was arising from changes in hopping distance and frequency, influenced by the phonon-induced trapping, rather than variations of the density of electronic mobile states.

Acknowledgments:

We greatly appreciate the inspiring discussions with Günter Reiter of the University of Freiburg, Germany. We also thank the financial supports by the National Science Council of Taiwan and the US Air Force Office of Scientific Research through the Taiwan–US Air Force Nanoscience Initiative Program (AOARD-094024, -104055, and -114055).

References

1. M. E. Raikh, I. M. Ruzin, in *Mesoscopic Phenomena in Solids*, Vol. 30, edited by B. L. Altshuler, P. A.Lee, and R. A.Webb (Elsevier, New York, 1991), p315.
2. Z. H. Wang, E. M. Scherr, A. G. MacDiarmid, A. J.Epstein, *Phys. Rev. B.* **1992**, 45, 4190.
3. M. Fox, Optical Properties of Solids: Oxford University Press, New York, 2001.
4. F. Laquai, G. Wegner, H. Bässler, *Phil. Trans. R. Soc. A* **2007**, 365, 1473.
5. J. W. Van der Horst, P. A. Bobbert, M. A. J. Michels, H. Bässler, *J. Phys. Chem.* **2001**,

114, 6950.
6. T. Guillet, J. Berrehar, R. Grousson, J. Kovensky, C. Lapersonne-Meyer, M. Schott, V. Voliotis, *Phys. Rev. Lett.* **2001**, 87, 87401-1.
7. P. Prins, F. C. Grozema, J. M. Schins, T. J. Savenije, S. Patil, U. Scherf, and L. D. A. Siebbeles, *Phys. Rev. B* **2006**, 73, 045204.
8. G. Weiser, S. Moller, *Phys. Rev. B* **2002**, 65, 045203.
9. B. K. Kuila, S. Malik, S. K. Batabyal, A. K. Nandi, *Macromolecules* **2007,** *40*, 278.
10. A. W. Musumeci, G. G Silva,; J. W. Liu, W. N Martens, E. R.Waclawik, *Polymer* **2007,** *48*, 1667.
11. H. Sirringhaus, P. J. Brown, R. H. Friend, M. M. Nielsen, K . Bechgaard, B. M. W. Langeveld-Voss, A. J. H. Spiering, R. A. Janssen, E. W. Meijer, D. M. de Leeuw, *Nature* **1999**, 401, 685.
12. H. G. O.Sanberg, G. L. Frey, M. N. Shkunov, M. M. Nielsen, C. Kumpt, *Langmuir* **2002** , 18, 10176.
13. F. Dinelli, M. Murgia, P. Levy, M. Cavallini, F. Biscarini, *Phys. Rev. Lett.* **2004**, 92, 116802-1.
14. Z. Bao, A. Dodabalapur, A. Lovinger, *Appl. Phys. Lett.* **1996**, 69, 4110.
15. H. Sirringhaus, N. Tessler, R. H. Friend, *Science* **1998**, 280, 1741.
16. A. Dodabalapur, L. Torsi, H. E. Katz, *Science* **1995**, 268, 270.
17. E. L. Granstrom, C. D. Frisbie, *J. Phys. Chem. B* **1999**, 103, 8842.
18. E. V. Emelianova, M. van der Auweraer, G. J. Adriaenssens, A. Stesmans, *Org. Electron.* **2008,** *9*, 129.
19. V. I. Arkhipov, P. Heremans, E. V. Emelianova, G. J. Adriaenssens, H. Bässler, *Appl. Phys. Lett.* **2003,** *82*, 3245.
20. M. C. J. M. Vissenberg, M. Matters, *Phys. Rev. B* **1998**, 57, 12964.
21. M. Nardone, V. G. Karpov, D. Shvydka, and M. L. C. Attygalle, *J. Appl. Phys.* **2009**, 106, 074503.
22. E. J. Meijer, C. Tanase, P. W. M. Blom, E. van Veenendaal, B. H. Huisman, D. M. de Leeuw, T. M. Klapwijk, *Appl. Phys. Lett.* **2002,** *80*, 3838.
23. J. J. Brondijk, F. Maddalena, K. Asadi, H. J. van Leijen, M. Heeney, P. W. M. Blom, D. M. de Leeuw, *Phys. Status Solidi* B **2011**, 1.
24. H. Shimotani, G. Diguet, Y. Iwasa, *Appl. Phys. Lett.* **2005,** *86,* 022104.
25. C. Tanase, E. J. Meijer, P. W. M. Blom, and D. M. de Leeuw, *Phys. Rev. Lett.* **2003**, 91, 216601.
26. T. Liang, Y. Makita, S. Kimura, *Polymer* **2001,** *42*, 4867.
27. Y. Miyoshi, K. I. Chino, *Jpn J Appl Phys* **1967,** *6*, 181.
28. S. Kwon, S. Han, *Molecul. Cryst. Liq. Cryst.* **2004,** 425, 77.
29. Z. C. Wu, Z. H. Chen, X. Du, J. M. Logan, J. Sippel, M. Nikolou, K. Kamaras, J. R. Reynolds, D. B. Tanner, A. F. Hebard, A. G. Rinzler, *Science* **2004,** *305*, 1273.
30. R. P. Raffaelle, B. J. Landi, J. D. Harris, S. G. Bailey, A. F. Hepp, *Mat Sci Eng B-Solid* **2005,** *116*, 233.
31. M. Zhang, S. L. Fang, A. A. Zakhidov, S. B. Lee, A. E. Aliev, C. D. Williams, K. R.; Atkinson, R. H. Baughman, *Science* **2005,** *309*, 1215.
32. F. R. Dubin, R. Melet, T. Barisien, R. Grousson, L. Legrand, M. Schott, V. Voliotis, *Nat. Phys.* **2006**, 2, 32-35.
33. J.-L. Bredas, R.Silbey, *Science* **2009**, 323, 348.
34. E. Collini, G. D. Scholes, *Science* **2009**, 323, 369.
35. K.-P. Tung, C.-C. Chen, P. Lee, Y.-W. Liu, T.-M. Hong, K. C. Hwang, J. H. Hsu, J. D. White, A. C.-M. Yang, *ACS Nano* **2011**, 5, 7296.
36. C. C. Chen, B. T. Chen, A. C.-M. Yang, Patents in application, Taiwan and US, 2011.
37. P. Lee, W.-C. Li, B.-J. Chen, C.-W. Yang, C.-C. Chang, Y. T. Chen, T. L. Lin, J. Tang, J.-H. Jou, et al., in submission.
38. P. Lee, *Enhancement of Photoluminescence in Conjugated Polymer Thin Film Induced*

by Molecular Packing Dewetting and Stretching, Master Thesis, National Tsing Hua University, 2011.
39. P. Lee, W. C. Li, Y. Chien, G. Reiter, A. C.-M. Yang, *Photoluminescence Influenced by Chain Conformation in Thin Conjugated Polymer Films by Spin Coating and Dewetting*. American Physical Society March Meeting Dallas, TX, USA, 2011; manuscripts in preparation.
40. A. Miller, E. Abrahams, *Phys. Rev.* **1960**, 120, 745.
41. J. Lindmayer, *J. Appl. Phys.* **1965,** 36, 196.
42. N. F. Mott, *J. Non-Cryst. Solids***1968,** 1, 1.
43. A. Miller, E. Abrahams, *Phys. Rev. Lett.* **1969**, 120, 745.
44. M. Pollak, J. J. Hauser, *Phys. Rev. Lett.* **1973,** 31, 1304.
45. G. Reiter, M. Hamieh, P. Damman, S. Sclavons, S. Gabriele, T. Vilmin, and E. Raphael**,** *Nat. Mater.* **2005**, 4, 754.
46. M. H. Yang, S. Y. Hou, Y. L. Chang, A. C.-M. Yang, *Phys. Rev. Lett.* **96**, 066105 (2006).
47. S. Al Akhrass, G. Reiter, S. Y. Hou, M. H. Yang, Y. L. Chang, F. C. Chang, C.F. Wang, A.C.-M. Yang, *Phys. Rev. Lett.* **2008**, 100, 178301.
48. Y. Chien, Y. L. Chang, A. C.-M. Yang, Molecular Strains and Packing Process of Long Polymer Chains in Ultrathin Films by Spin Casting, to be submitted.
49. T. M. Huang, *Electric Conductivity of Polymeric Nanolayers Grafted on Multi-Walled Carbon Nanotubes in Nanocomposites*, Master Thesis, National Tsing Hua University, 2010.
50. J.-Y. Lin, *Electric Conductivity of Polymer/Carbon Nanotubes (CNTs) Nanocomposites: CNT Surface grafting, p-p interactions, and Gold Nanoparticles adsorption effect*, Mater Thesis, Department of Materials Science and Engineering, National Tsing Hua University, Hsinchu, Taiwan, 2006.
51. A. P. Le, T.-M. Huang, P.-T Chen, A. C.-M. Yang, *J. Polymer Sci. Part B: Polym. Phys. Ed.* **2011**, 49, 581.
52. T. S. Lin, L. Y. Cheng, C. C. Hsiao, A. C. M. Yang, *Mater. Chem. Phys.* **2005,** *94*, 438.
53. C.-C. Hsiao, T. S. Lin, L. Y. Cheng, C.-C. M. Ma, A. C.-M. Yang, *Macromolecules* **2005**, 38, 4811.
54. C.-W. Lin, L. C. Huang, C.-C M. Ma, A. C.-M. Yang, C.-J. Lin, L.-J. Lin, *Macromolecules* **2008**, 41, 4978.
55. C. W. Lin, A. C.-M. Yang, *Macromolecules* **2010***,* 43, 6811.
56. D. Stauffer, A. Aharony, *Introduction to Percolation Theory,* Taylor and Francis: 1994.
57. M. Weber, M. R. Kamal, *Polymer Composites* **1997**, 18, 711.
58. C. Gau, C.-Y. Kuo, H. S. Ko, *Nanotechnology***2009**, 20, 395705**.**
59. B. Philip, J. N. Xie, A. Chandrasekhar, J. Abraham, V. K. Varadan, *Smart Materials & Structures* **2004,** *13*, 295.
60. Y. K. Han, Y. J. Lee, P. C. Huang, *J. Electrochem. Soc.* **2009**, 156, 37.
61. C. Y. Li, E. T. Thostenson, T. W. Chou, *Appl. Phys. Lett.* **2007,** *91*.
62. M. S. Fuhrer, J. Nygard, L. Shih, M. Forero, Y. G. Yoon, M. S. C. Mazzoni, H. J. Choi, J. Ihm, S. G. Louie, A. Zettl, P. L. McEuen, *Science* **2000,** *288*, 494.
63. F. C. Chiu, J. J. Wang, J. Y. Lee, S. C. Wu, *J. Appl. Phys.* **1997,** *81*, 6911.
64. M. Estrada, I. Mejia, A. Cerdeira, B. Iniguez, *Solid-State Electronics* **2008,** *52*, 53.
65. B. I. Shklovskii and A. L. Efros, *Electronic Properties of Doped Semiconductors* (Springer, Berlin), 1984.
66. A. V. Tartakovskii, M. V. Fistul', M.E. Raikh, and I. M. Ruzin, *Sov. Phys. Semicond.* **1987**, 21, 370.
67. A. Nitzan, *Annu. Rev. Phys. Chem.* **2001**, 52, 681.

Supplemental Section:

Table 1. The reaction condition of CNT-P-4 and CNT-P-8

Sample	$FeCl_3$	Solvent	Reaction Time
CNT-P-4 (3.6 nm)	0.32g	1% acetonitrile + 99% chloroform	30 minutes
CNT-P-8 (8.3 nm)	0.64 g	100% chloroform	24 hours

Table 2. The ρ_0, φ_c and t of the nanocomposites

Sample	$\rho_{0,V}$ (Ω-cm)	$_{c,V}$ (wt%)	t_V	$\rho_{0,H}$ (Ω-cm)	$_{c,H}$ (wt%)	t_H
MWCNT	9.2×10^{1}	8.1	3.4	4.9×10^{-2}	0.005	3.2
CNT-P-2 (2.1nm)	4.2×10^{5}	9.1	3.4	1.9×10^{2}	0.001	3.2
CNT-P-4 (3.6nm)	4.5×10^{6}	9.4	2.3	2.0×10^{3}	0.003	3.2
CNT-P-8 (8.3nm)	7.1×10^{8}	9.4	1.4	8.0×10^{5}	0.001	2.3

Table 3. The R_c and ρ_{P3HT} for various P3HT coating thicknesses

Coating Thickness	L_z/L_{xy} (m/ m)	n_z/n_{xy}	$\langle l_{i,z}\rangle/\langle l_{i,xy}\rangle$ (m/ m)	R_C (Ω)	ρ_{P3HT} (Ω-cm)
0 nm	25/1000	610/785	0.041/1.96	1.2×10^{4}	N/A
2.1 nm	25/1000	658/785	0.038/1.96	5.0×10^{7}	7.0×10^{2}
3.6 nm	25/1000	676/785	0.037/1.9	5.3×10^{8}	5.5×10^{3}
8.3 nm	25/1000	424/785	0.059/1.96	1.3×10^{11}	1.1×10^{6}

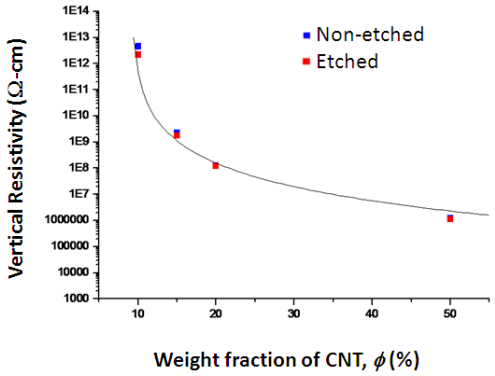

Figure S1: Electric resistivity measurements in the vertical directions of the nanocomposite films containing CNT-P-2 versus the CNT weight fraction . (Etching condition: 60 W Oxygen plasma for 10 minutes, etching depth ~60nm)

3. Massive Enhancement of Photoluminescence of Conjugated Polymer by Dewetting-Induced Molecular Stretching

The photoluminescence (PL) of a conjugated polymer, poly[2-methoxy-5-((2'-ethylhexyl)oxy)-1,4-phenylenvinylene] (MEH-PPV), manifests an enormous enhancement when the polymer film dewets on a surface. The enhancement arises mainly from stretching of the conjugated polymer by molecular recoiling toward equilibrium conformations. The dewetting polymer chains, eventually spreading thinly over the "exposed" substrate forming a residual layer (~2-3 nm) or collected into the droplets, emit light up to several folds stronger than the non-dewetted. A large blue shift of the emissions is accompanied with the dramatic PL increases, signifying a stretching-induced reduction of conjugation length in the

renewed chain entanglement network of the dewetting polymer. Furthermore, exciton quenching when conjugated polymers contact narrow-bandgap substrates can be switched off by the molecular stretching, indicating that mechanical stress states are closely related to the formation and the subsequent behavior of the photo-induced species. We attribute these observations to the reduction of phonon-exciton coupling in the molecularly constrained conjugated polymer chains resulted from the long-distance material redistribution. This unique approach of molecular stretching for dramatic efficiency enhancement is compatible with the existing fabrication methods of polymer-based diodes and solar cells.

Introduction

Ultrathin films of conjugated polymers (CPs) have attracted extensive interests, owing to the low cost, unique mechanical properties, tunable optoelectronic behavior that make them highly appealing for lighting, energy harvest, and microelectronics [1-5]. The practical applications of CPs, however, have been bottlenecked with their low optoelectronic efficiencies. Recently, new evidence emerged indicating that proper controls over the molecular conformation and the molecular stresses of the molecules may provide effective ways to revamping the efficiency landscape [4-11]. Along the same line, hereby we report an astonishing enhancement of photoluminescence (PL) and the fundamental modifications over the optoelectronic behavior of CP chains which were molecularly constrained by extensive shearing on partially wettable surfaces [10-13].

The low quantum efficiencies of CPs are believably due to self-trapping of the photo-excited species [7-9,14-18] via strong electron-phonon coupling [4,5,14-17] that obstructs radiative pathways. The entrapment results from the time-integrated chain vibrations swayed by the local electric fields created from the excited states, creating molecular deformations that block the coherent transport. Since CPs are intrinsically softer than the inorganic crystalline counterparts, the electron-phonon interactions are much more prevalent in these soft chain-like molecules. However, the coupling may be made more difficult by putting the molecule under a tension. Recently, dramatic enhancement of PL efficiency was reported in isolated MEH-PPV molecules when they were stretched to large strains [9], supporting the efficient interactions between mechanical deformations and optoelectronic behavior in this class of materials. Further on, as a corollary of the interactions, substantial variations in how the excitons form, move, and annihilate are expected to occur when the molecules are stretched.

Along a separate line, significant residual stresses are operative when CPs are packed into thin solid films below their characteristic molecular sizes of radius of gyration (R_g) for optoelectronics applications [19-23]. Dewetting takes place when the films contact heat or solvent vapor to lower the free energy [10-13,24-27]. During the process, long-distance molecular movements that accompany extensive stress release ultimately produce polymer droplets and a residual layer on the substrate. Chain mixing inevitably occurs when the confined molecules recoil toward the thermal equilibrium, ushering in topological renewal of the chain entanglement network. In the residual layer, the adsorbed molecules are sheared and confined to the substrate with chain orientation in the direction of the dewetting front similar to “molecular combing” of DNA stretched with a receding meniscus. On the other hand, in the droplets, the polymer molecules have traveled hundreds of R_g‘s in extensively altered chain entanglements under a complicated but mostly tensional stress state. Substantial chain stretching has occurred during the dewetting.

Here, we report that a dewetting process can produce highly stretched states of conjugated polymers which yielded a massive increase of PL and fundamental alterations of the optoelectronic properties. This approach, compatible with the microelectronic processes, may lead to the fabrication of efficient optoelectronic devices based on polymers.

Experimental Section

The polymer poly[2-methoxy-5-((2'-ethylhexyl)oxy)-1,4-phenylenevinylene],

MEH-PPV, was purchased from Sigma-Aldrich Chemical Co., with a molecular weight M_w~250,000 g/mol and with polydispersity (M_w/M_n) around 5. Low molecular weight polystyrene (PS) was bought from Pressure Chemical Co. with a molecular weight of M_w = 2 kg/mol and $M_w/M_n \leq 1.06$. A solvent blend of equal-parted toluene (HPLC/SPECTRO, Tedia), tetrahydrofuran (THF, anhydrous, Tedia), and cyclohexanone (GC grade, Sigma-Aldrich) was used to make the polymer solutions for preparing the film samples. Thin films of pristine MEH-PPV films and the blend of MEH-PPV in PS with the MEH-PPV fraction (c) between 0 and 25% were prepared for the experiments.

The solution was stirred slowly at 50°C for 12 - 24 hours and filtered (0.45 μm pore size) to remove any non-dissolving particles. The polymer solution was then spin-casted on a 1 cm × 1 cm substrate, resulting in smooth and uniform films. By adjusting the spin-speed, the film thickness ( ) was controlled at 10, 20, 30, 40, and 60 nm. The substrate was a bare silicon wafer that came with a thin native oxide layer of about 2 nm. In certain experiments where dewetting was to be facilitated, a thin layer of polydimethylsiloxane (PDMS: Sylgard 182, Dow Corning) was coated, by spin coating and then cured at 130°C, on the silicon wafer before the deposition of polymer film. The thickness of resulting PDMS layer was controlled to be around 3 nm for the pristine MEH-PPV films and less than 1 nm for the films of MEH-PPV/blends. Substrates of silica (premium cover glass, Fisherfinest) and thick silicon oxide coating (~500 nm) grown on silicon wafer were also used for examining the effect arising from a built-in voltage at substrate surface.

After preparation, the samples were always protected in aluminum foil wrappings before being tested. Some control samples were prepared in a glove box (MBraun, Germany) but results were essentially identical to that prepared in the ambient conditions.

The films were subsequently annealed in a vacuum oven at a temperature ranging between 100 - 130°C, during which the film morphology and the luminescence spectra were monitored and recorded. To minimize the effect of transient heating and cooling at the beginning and end of each annealing process, the sample was used only for one annealing time. Optical microscopy and atomic force microscopy were used to visualize the film morphology. PL spectra were obtained with a fluorescence spectrometer (Perkin Elmer). The dewetted film was also examined by utilizing a scanning near-field optical microscope for PL mapping. An confocal optical system consist of laser sources (473 and 632.8 nm), an inverted optical microscope (Olympus IX71), and a detector (Princeton Instrument, SP2300) in an optical circuit that integrated with an atomic force microscope (AFM) (Catalyst II, Brucker) served as a micro-PL for probing the fluorescence property of small areas of the samples. In order to explore the thickness of the residual monolayer of dewetted films, x-ray reflectivity method using the synchrotron radiation (National Synchrotron Radiation Research Center, . 0.154982 nm) was employed. The specular reflectivity was measured and the resulting curves were fitted to a multilayered model following the Abeles formulation [28-29]. From this fitting, the fine structure of the dewetted film was obtained.

Results and Discussions

Dewetting of Polymer Films

During spin coating, the giant molecules of polymers quickly transformed within a short elapse of time as solvent evaporated rapidly from isolate fully solvated molecules to drying coil aggregates packed densely into the confining thin condensed film. The substrate provided not only a template for supporting the film but also a source of van der Waals forces interacting with the solvent and polymer molecules during the film formation process that strongly influenced solvent evaporation and the evolution of molecular packing [11]. When annealed at a temperature between 100 and 130°C for a period of incubation, the films started to dewet by the growth of small pinholes that grew and later on coalesced evolving into droplets (Fig. 1a), to release the large residual stresses [19-23]. The required annealing times for the start and completion of the dewetting were significantly longer for greater film thicknesses ('s) or higher MEH-PPV concentrations. For films below . ~10 nm, the

instability was driven by the mechanism of a spinodal mode [28] without obvious incubation annealing and pinhole formation.

During the topographic evolution that finally formed droplets, a “residual layer” was observed on the “exposed” substrate. The thickness of this residual layer was determined by x-ray reflectivity using synchrotron radiation as well as AFM topographic analysis on scratched samples. A single layer model was fitted to the reflectivity curves (Figs. 1c and 1d) indicating that there was a continuous residual layer remaining within of the fully dewetted films on all substrates. Its thickness, although decreasing with dewetting was almost independent of . when fully dewetted. For a typical sample of 20 nm 25% MEH-PPV blend film, it decreased from ~3.9 ±0.2 nm as the hole just touched the substrate to the terminal value of ~2.1±0.2 nm (Fig. 1c) when the droplet pattern was already formed. The data were consistent with the AFM results of the difference between . and the hole depth(Fig. 1b). The residual layer thickness tended to increase slightly for higher MEH-PPV contents.

(a)

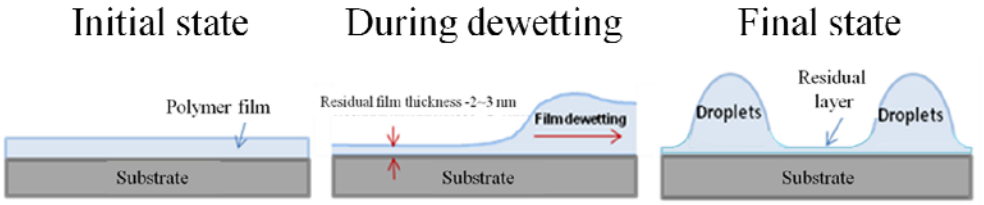

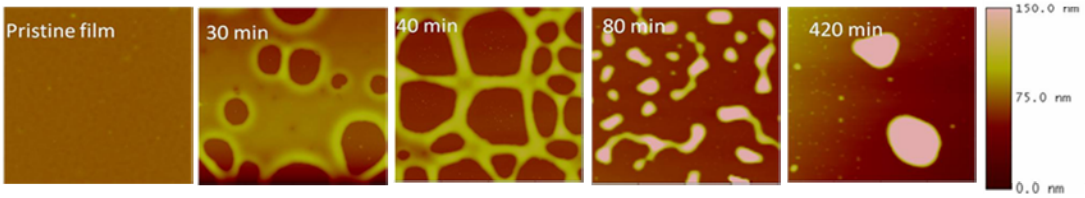

(b) (c)

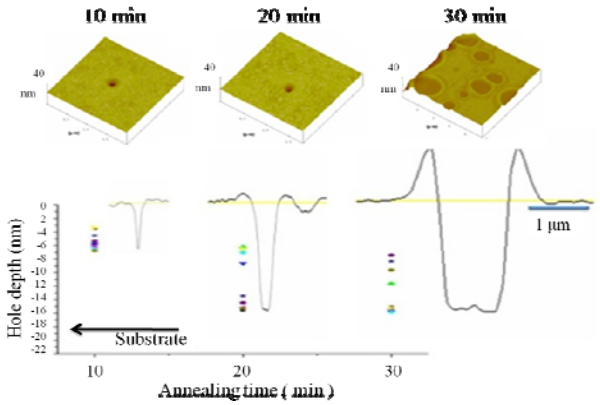

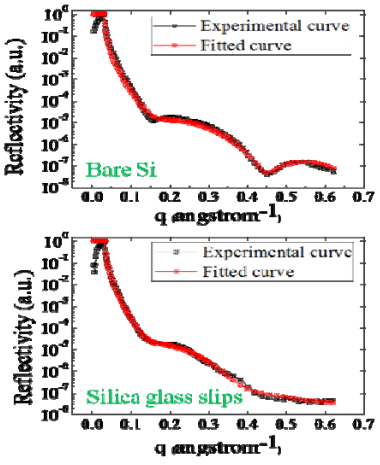

d)

Layers		Film thickness (A)		SLD (10^{-6} A^{-2})		Roughness (A)	
		Fitting	AFM	Fitting	Calculation	Fitting	AFM
Droplets	Wafer	2023.4	1949.7 ± 236.0	0.60	0.70	255.4	251.6 ± 6.1
	O-wafer	2000.7	1938.1 ± 195.6	0.30	0.71	251.07	244.5 ± 6.8
	Glass	1520.0	1524.1 ± 164.6	0.40	0.94	253.3	252.2 ± 3.2
Residual film	Wafer	21.19	Difficult to measure	5.85	8.27	1.07	4.17 ± 0.7
	O-wafer	19.34	Difficult to measure	5.56	8.26	1.48	3.89 ± 0.6
	Glass	22.67	Difficult to measure	6.99	8.02	4.39	5.45 ± 0.7

Figure 1. (a) Schematic depiction of the dewetting process and the topographic evolution of dewetted thin films (c = 20%, $_{.}$ = 20 nm) by AFM. (b) The cross-sections of the dewetting holes that show the existence of a residual polymer layer at the bottom of the opening in a = 20 nm film. (c) The residual layer thickness was determined from x-ray reflectivity to be 2.1 and 2.3 nm, respectively, for films (c = 20%, $_{.}$ = 20 nm) on bare silicon (top) wafers and silica glass slip (bottom). d) X-ray reflectivity data (MEH-PPV/PS blend films, = 20 nm).

Toward the final stage of the dewetting, the droplets grew into a height up to around several hundred nm and extended laterally tens microns. Their sizes, however, were strongly dependent on $_{.}$ and the substrate. Although conspicuous under the AFM surveys, the droplets rose on the sample topography mildly with a surface angle ranging approximately from 5 to 10 degree. These droplets were removed when the dewetted films were washed in the solvent, whilst the residual layer remained, illustrating the large difference in substrate adhesion of the droplets and the residual layer. The residual layer obviously was confined strongly to the substrate.

PL of Dewetting Films

During dewetting the PL of the films underwent dramatic changes. The PL spectra at various annealing times leading to dewetting were shown in Fig. 2a for samples of thicknesses from 10 to 30 nm on silicon or glass substrate. In the initial incubation period, the still intact films manifested a significant decrease of PL intensity along with a red shift (from 565 to 585 nm for the 20 nm MEH-PPV/PS films, Fig. 2a). The PL intensity was taken from the peak normalized to that before annealing. The data indicate that when no large scale molecular motions were incurred the stress relaxation induced by annealing (intact-film relaxation) had caused increases of conjugation length, amid which chain aggregation was also occurring as hinted by the decrease of PL [9].

However, once pinholes emerged to commence the dewetting, a new PL peak appeared at a wavelength blue shifted relative to the original emission. The new peak, remained approximately unchanged in position throughout the dewetting at ~543 nm for the 20 nm MEH-PPV/PS films, eventually overwhelmed the PL emission, bringing the PL intensity to a increase of more than 10 folds for $_{.}$ = 20nm on silicon wafer. Separate experiments of dewetting triggered by immersing the films in solvent vapor (solvent annealing) [12] produced almost identical results, clearly indicating that the new PL peak was not arising from thermal degradation but from chain movements of the dewetting films. The exact wavelengths of the red shifted peak and the blue shifted peak depended on the MEH-PPV content, , and substrate interactions, as will be detailed later. In contrast to the red shifting observed for the annealed intact films, the blue shifts of PL during dewetting indicate the significant decrease of conjugation length of the MEH-PPV molecules that were dragged in long distances. Clearly, chain recoiling in the receding films had introduced a renewal of chain packing that saw a substantial increase of effective chain entanglement density causing the reduction of conjugation length.

Generally, the blend films dewetted faster than the pristine MEH-PPV films due to the plasticizing effect of the low molecular weight polystyrene. In addition, an even stronger enh ancement PL compared to the pristine MEH-PPV was observed.

In further details, the PL spectra before dewetting were analyzed by Gaussian curve fitting the wavelengths of the maximum emissions resulting from intra-chain and inter-chain transitions, to be 565 nm and 595 nm, respectively, in good agreement with those reported elsewhere [30]. The spectra of the dewetting films were then analyzed by assuming unchanged wavelengths of these emissions but adding the contribution of a new peak (at 543 nm for the 20 nm films) that clearly was arising from molecular stretching during dewetting. Evidently, in the course of dewetting the intensity of the new increased rapidly while the original intrachain and interchain emissions underwent only relatively smaller changes. Such behavior was observed for all thicknesses of the MEH-PPV films.

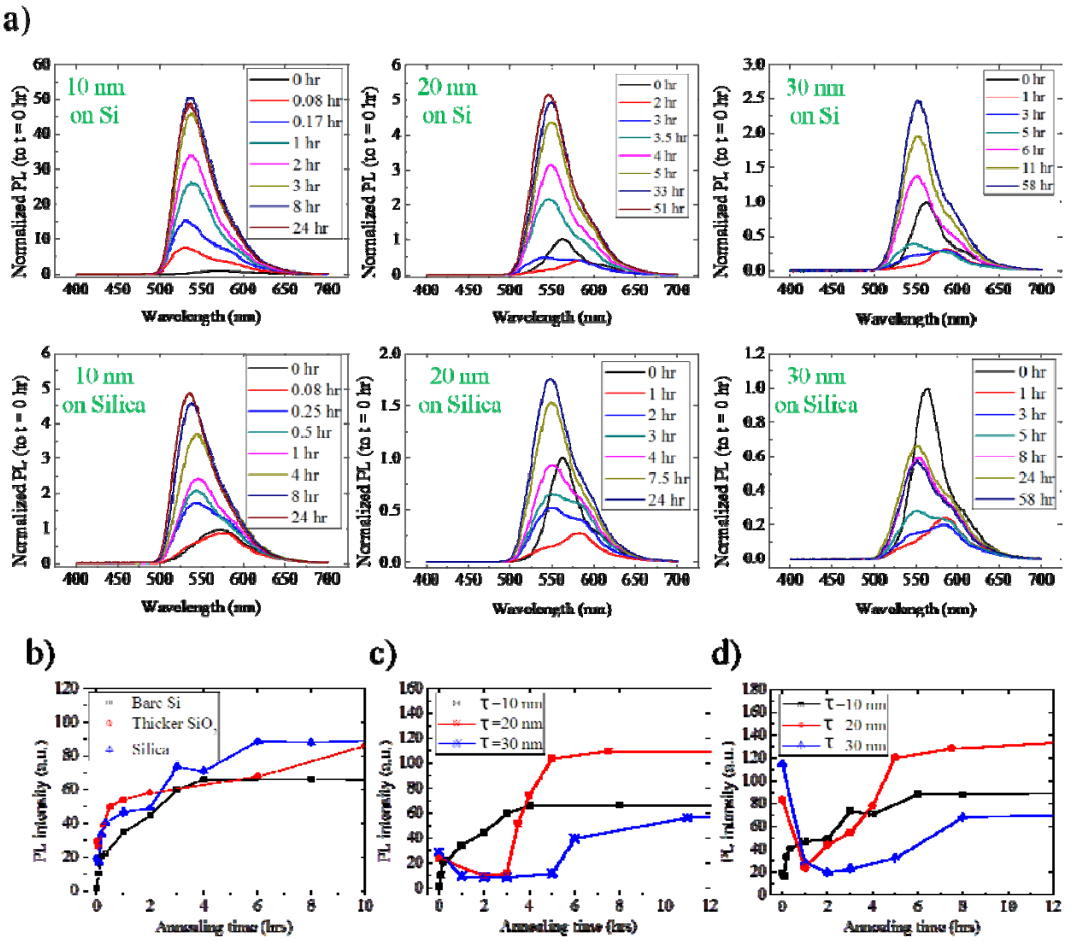

Figure 2. The temporal evolution of the films (c = 15%) as influenced by dewetting: a) PL spectra of various thicknesses on bare Si and silica, b) PL intensities as influenced by the substrate (= 10 nm), c) the PL intensities for various thicknesses on bare silicon, and d) the PL intensities of various thicknesses on silica.

Effects of Film Thickness and Substrate

To analyze the effects of film thickness and film-substrate interactions, the temporal evolution of the PL intensities during dewetting was illustrated in Fig. 2b (for = 10 nm on silicon, thick silicon oxide, or silica) and Figs. 2c and 2d (for = 10, 20, and 30 nm on silicon or silica). The effect of intact-film relaxation was found to decrease as thickness decreased. This obviously was due to shortening of the incubation prior to the dewetting, resulted from the increase of molecular recoiling [18-22] and capillary forces [25,26]. For the thinnest films of = 10 nm, the effect of intact-film relaxation was difficult to observe because dewetting took place almost instantaneously upon annealing in the unstable films to initiate the stage of PL enhancement with the PL blue shifts.

In contrast, the effect of molecular stretching observed after the start of dewetting increased with decreasing thickness where the driving forces of molecular recoiling and capillary forces rose. The PL enhancement (relative to the PL intensity prior to annealing) in the fully dewetted samples dropped from ~50 folds for = 10 nm, to ~5 folds for = 20 nm, and to ~2.5 folds for . = 30nm when the films were on silicon substrate. For the films on the silica substrate, the enhancement decreased from ~5 folds for = 10 nm, to ~1.8 folds for = 20 nm, and to ~0.6 folds for = 30 nm. The effect of molecular stretching for the thick films (= 30 nm) on silica was so small that it registered no enhancement, and in fact the PL of the fully dewetted films was actually lower, in comparison to that prior to

annealing. It, however, was still significantly greater than the PL of stress relaxed intact films by a factor of ~3. By the same token, on the PL blue shifts by the molecular stretching, the new peak emerged at ~554 nm for = 30 nm, ~543 nm for = 20 nm, and ~535 nm for = 10 nm (for the 25% MEH-PPV films), strongly indicating that the molecular stretching was more efficient in thinner films where chain re-entanglement was also more prevalent.

It is very important to note that a large effect from the substrate on the PL properties of the polymer films was observed. The PL intensities of films thinner than 50 nm were found to reduce dramatically when the films were coated on silicon substrate as compared to those on the substrate of silica or thick silicon oxide. This effect was arising from the quenching effect on the photo-induced excitons migrating near the film-silicon interface where a large electric field arising from Fermi-level alignment tore the excitons apart and annihilated them [23]. For the substrates with bandgaps greater than that of the conjugated polymer, e.g., silica and thick silicon oxide, such effects did not exist because the built-in electric fields at the interface were not dissociative for the excitons. The dewetting, nevertheless, induced dramatic increases of the PL intensity, by a factor of 4-5 for films on silica and thick silicon oxide. Therefore, the dewetting induced PL enhancement observed in the films on silicon was the result of the molecular stress effects on the PL enhancement as well as that on this quenching effect. Since the silica substrate was immune to this quenching effect, the dewetting induced effect on silica can be used as a reference for analyzing the data on silicon. From Figs. 2a-d, it is clear that the dewetting induced PL enhancement in the films on silica was much smaller than that on silicon, e.g., 50 folds (on silicon) vs 5 folds (on silica) for = 10 nm. Furthermore, the PL intensities of the final fully dewetted samples were approximately independent of the choice of the substrate [11] (not shown). The information indicates that the quenching effect on the non-dewetted films on silicon has contributed significantly to the observed very large enhancement factor because the PL intensities were very low in the beginning. It also indicates that molecular stretching may switch off the exciton quenching effect. This conclusion, as will be verified further by the confocal micro-PL data in the following, contains very important meaning for exciton formation, transport, and annihilation in conjugated polymers in the light of electron-phonon interactions.

Confocal Micro-PL

To analyze the respective components of the PL spectrum contributed from the various structrual features of the dewetted film, the local PL spectra of the as-cast films, the stress-relaxed intact films, the droplets and the residual layer on the fully dewetted films were collected (Fig. 3a) uisng a confocal micro-PL spectrometer (spot size ~1 micron) coupled with an AFM for precision positioning. The peak-shifts of the micro-PL spectra were reliable for fingerprinting the respective contributors to the investigated PL enhancements. The intensities, however, were used with cautions as they were highly sensitive to the surface curvatures of the surveyed spots. Therefore, only planar objects, such as films or residual layers, were compared for the intensities.

The decrease of PL emission and the associated red shifts in the stress relaxed intact films observed by using the bulk PL spectrometer were replicated under the micro-PL. In addition, the feature blue shifts were observed in both the spectra from the residual layer as well as the droplets. The PL from the droplets, nevertheless, showed a larger shift than that of the residual layer, indicating that the emerging new peak (Fig. 2a) came from both the residual layer and the droplets and that large molecular deformations had taken place in both the residual layer and the droplets. It also indicates that, renewal of chain entanglements proceeded more in the droplets than in the residual layer, which is fully comprehensible because chain mixing was difficult in the molecularly thin, substrate-adhering residual layer. Furthermore, the droplets varied widely in sizes and hence contained polymer chains stretched (and realxed) to various degrees; they also manifested a relatively broad range of PL emission intensities, consistent with the effect of molecular stress. Nonetheless, due to

the convex topography of the droplet, the PL intensity collected in the confocal system were believedly substantially lower than that of identical mechanical history but of a planar topography.

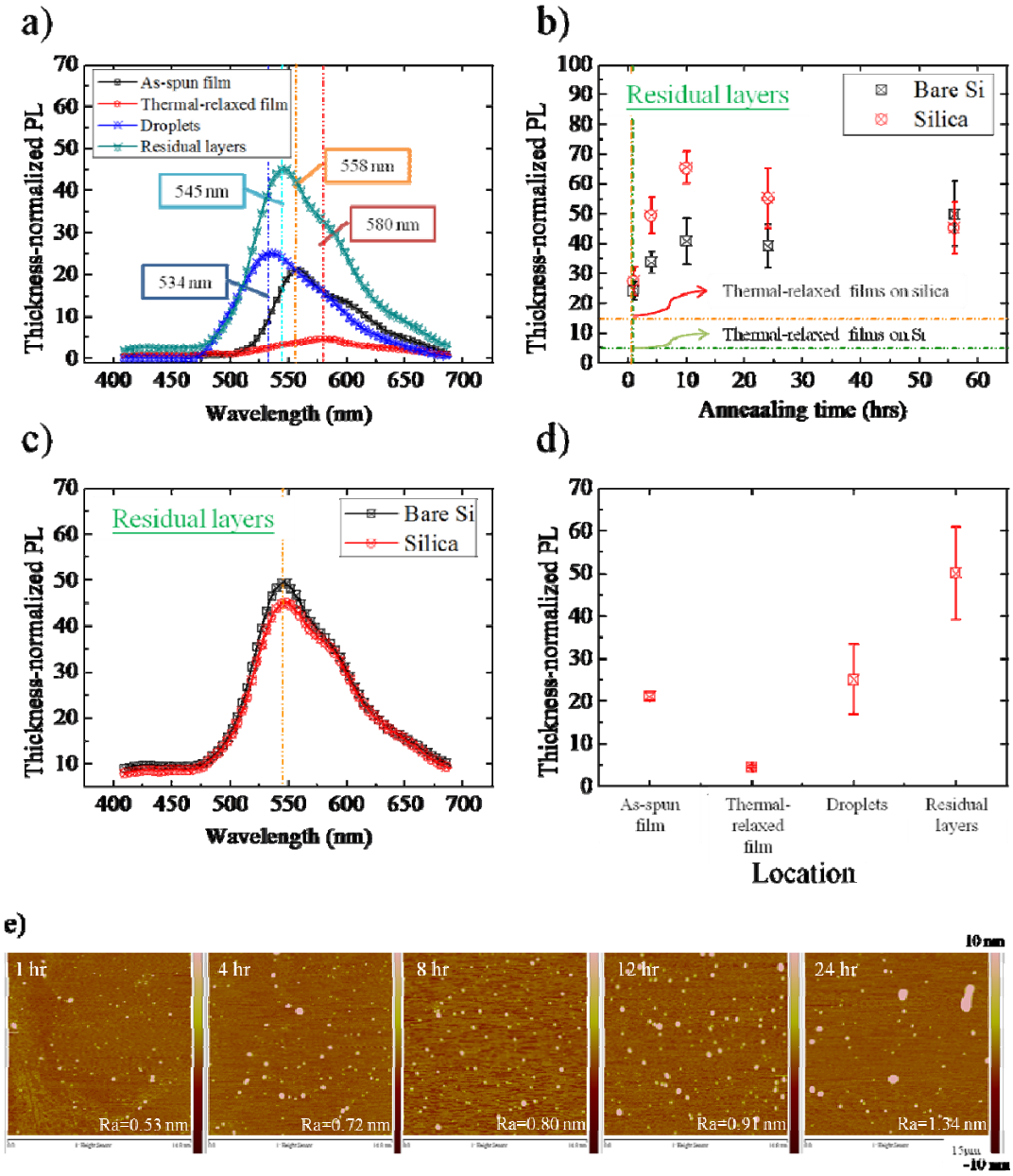

Figure 3. For a thin film (c = 15%, = 20 nm): (a) The local PL spectra of the dewetted fil m, (b) Temporal variation with dewetting of the PL intensities from the residual layers on bar e silicon and silica, c) the PL spectra of the fully dewetted residual layers on bare silicon and silica, d) the comparison of averaged local τ -normalized PL intensities from the as-cast film, thermally relaxed films, droplets, and the re sidual layer, and e) the temporal evolution of the topography by AFM of the residual layer on bare silicon.

The PL efficiency (obtained by normalizing the peak PL intensity to the local thickness) of the residual layer was found to increase in general with dewetting (Fig. 3b). Interestingly, exciton quenching was already switched off in the residual layer on silicon at the early stage of dewetting, as seen from the increased PL intensity relative to that of the

as-spun film on silica (Fig. 3b). It is important to note that the PL spectra from the residual layers on silica and silicon were almost identical (Fig. 3c). The absence of exciton quenching indicated that charge recombination was extremely efficient such that essentially no excitons had ever made it to the interface even at a maximum distance of ~2 nm from the substrate. Evidently, the state of molecular stress may dramatically alter the formation, structure, and properties of excitons. While the enhancment is expected to be greater for thinner films, for τ = 20 nm the final PL efficiencies of the residual layers were about ~10 times greater than that from the thermally realxed intact films, indicating the strong effect of molecular stresses. Toward the final stage of dewetting, the PL spectra of residual layers on various substrates tended to merge together although different realxation pathways were taken[31] that demonstrated somewhat varied evolutions of the PL intensity (Fig. 3b) in associatation with the topography changes (Fig. 3e).

The stressed MEH-PPV molecules collected in the droplets contributed substantially to the dewetting-induced PL enhancement with just as prominent enhancement as demonstrated by the residual layer. Since the residual layer accounted for only 10% of the total mass of the films, the majority of the enhanced PL came from the droplets. This was reflected in the confocal micro-PL data of the significnatly enhanced intensity (Fig. 3d) that signified chain stregching. The fact that the blue shift was greater in the droplets than that in the residual layers stemed from the greater extent of molecular mixing in droplets than the residual layer. Furthermore, as manifested by the solvent washing experiment mentioned previously, the droplets, however, did not adhere as strongly to the substrate as the residual layer, indicating that the electron-phonon interactions in the bottom layer of the droplets, where compressive rather than tensional stresses were present, was not as effectively suppressed as that in residual layer. This will provide opportunities of exciton quenching and decreasing the observed PL efficiencies of the droplets.

In fact, the existence of the residual layer provided the required anchoring for strong shear to take place in the transported polymer molecules. The polymer chains were either displaced into the droplets or, due to the large substrate adhesive effect, spread and clogged on the substrate. Similar to “molecular combing”, we suppose that MEH-PPV chains get partially adsorbed onto the substrate and are subsequently stretched in the flow field generated by the retraction dewetting front. We note that the enhancement effect was generally lower in the “solvent annealing” experiments, which was attributed to the reduced adsorption and increased chain relaxation in the solvent-rich environment [10-12]. The formation of the residual layer obviously was strongly influenced by the specific interactions between the dewetting polymer films and the substrates and is well predicted by the minimum thickness h^* that corresponds to the capillary surface potential minimum [27]. Continuous evolution of the topography of the residual layer indicates that the equilibration of the thin molecular layer took long time and in fact may trigger a second stage of dewetting of this residual layer, as manifested by surface coarsening and bump formation in Fig. 3e and as suggested previously by other authors [31].

The extraordinarily large optoelectronic enhancements induced by dewetting was attributed to the effective molecular constraints from the molecular stresses. When the conjugated polymer chains are stretched, self-trapping of excited electronic states was significantly depressed due to increased difficulties to accumulate local deformation for the entrapment to produce much more efficient charge recombination for luminescence. The stress-induced enhancement of the optoelectronic efficiencies was observed not only in the dewetted films, but also in the uni-axially stretched polymer films that contained conjugated polymers [9]. In addition, in the mesoscopic confined polymer films, the electric conductivity was found to increase more than 5 orders of magnitude as the film thickness decreases to ~2nm [32]. All these evidence supports that energy dissipations are substantially reduced as the electron-phonon coupling is suppressed in the molecularly constrained CP chains.

The blue shift of the PL emission arising from dewetting obviously indicates the

reduction of conjugation lengths of the CP chains in the dewetting films and droplets. Molecular stretching at the newly formed chain entanglement points during dewetting was attributed to the reduction of conjugation length and the blue shift. Since similar blue shifts were observed during the early stage dewetting of multilayer thin films of PS on top of very thin neat MEH-PPV films when only stress transfer from PS to MEH-PPV films was possible [13], the length scales of the mechanism causing the blue shifts are comparable to the contour lengths of chain sections between adjacent chain entanglements.

Conclusions

The shear flows driven by recoiling of the large non-equilibrated polymer chains and the long range van der Waals interactions during dewetting of ultrathin films that contained conjugated polymers gave rise to dramatic increases of the PL efficiencies. The enhancement of PL is accompanied by the formation of a new emission peak, emerging at a wavelength a blue-shifted relative to the original film emission. The blue shifted peak, signifying the extensive molecular mixing by the recoiling chains during dewetting, was attributed to the highly stressed conjugated polymer chains in the dewetted films and may eventually overwhelm the total emission to give a PL enhancement up to many folds. Confocal micro-PL spectroscopy revealed that both the droplets and the thin residual layers on the "exposed" substrate contained polymer chains that were highly stretched and optoelectronically enhanced. With the large efficiency enhancement, the stretched chains manifested no exciton quenching even at ~2nm proximity within a highly dissociative interface. This indicates that when subject to varied states of molecular stresses, the formation, fine structures, and properties of excitons in conjugated polymers may be altered and controlled. The large optoelectronic enhancement is attributed to the reduced phonon-exciton coupling of the molecularly constrained conjugated polymer chains.

Such large optoelectronic enhancement in thin films induced by dewetting may find useful applications in the energy and lighting devices as the thin film preparation and annealing processes involved are fully compatible with the current prevailing technology for microelectronics and display industries.

Acknowledgements

The authors sincerely thank Drs. C. T. Yuan and P. K. Wei of Academia Sinica (RCAS) of Taiwan for their contributions on, respectively, single molecule spectroscopy and scanning near-field optical microscopy. We also appreciate the instructive discussions with the late Prof. Paul Barbara of University of Texas at Austin, U.S.A. and Dr. Mark Geoghegan of University of Sheffield, U.K. The work is supported by National Science Council of Taiwan (NSC 98-2120-M-007-010-; NSC 96-2628-E-007-020-MY3) and grants from the US Air Force (AOARD-084125, -094024, -1014055) under the US Air force-Taiwan NSC Nanoscience Initiatives.

References

[1] G. Gustafsson, Y. Cao, G. M. Treacy, F. Klavetter, N. Colaneri, and A. J. Heeger, *Nature* **357**, 477(1992).
[2] D. Braun, A. J. Heeger, *Appl. Phys. Lett.* **58**, 1982 (1991).
[3] M. Berggren, O. Inganas, G. Gutafsson, J. C. Carlberg, J. Rasmusson, M. R. Andersson, et al, *Nature* **372**, 44 (1994).
[4] G. He, Y. Li, J. Liu, Y. Yang, *Appl. Phys. Lett.* **80**, 22 (2002).
[5] T.- Q. Nguyen, V. Doan, B. J. Schwartz, *J. Chem. Phys.* **110**, 8 (1999).
[6] P. F. Barbara, A. J. Gesquire, S.-J. Park, Y. J. Lee, *Acc. Chem. Res.* **38**, 602 (2005).
[7] J. Yu, R. Lammi, A. J. Gesquiere, P. F. Barbara, *J. Phys. Chem. B* **109***,* 10025 (2005).
[8] J. Yu, D. Hu, P. F. Barbara, *Science* **289**, 1327 (2000).
[9] K. P. Tung,; C. C. Chen, P. Lee, Y. W. Liu, T. M. Hong, K. C. Hwang, J. H. Hsu, J. D. White, A. C.-M. Yang, *ACS Nano* 5, 7296-7302(2011); K. P. Tung, *Master Thesis* 2008,

Department of Materials Science and Engineering, National Tsing Hua University, Taiwan.
[10] C. W. Yang, *Master Thesis* 2006, Department of Materials Science and Engineering, National Tsing Hua University, Taiwan. B. J. Chen, *Master Thesis* 2010, Department of Materials Science and Engineering, National Tsing Hua University, Taiwan.
[11] P. W. Lee, W. C. Li, Y. Chien, G. Reiter, A. C.-M. Yang, "Photoluminescence Influenced by Chain Conformation in Thin Conjugated Polymer Films by Spin Coating and Dewetting", 2011, March Meeting of American Physical Society (Y44-10), Dallas, TX, U.S.A., manuscript in preparation; P. Lee, *"Enhancement of Photoluminescence in Conjugated Polymer Thin Films induced by Molecular Packing, Dewetting, and Stretching"*, Master Thesis, 2011, National Tsing Hua University, Taiwan.
[12] B. J. Chen, "Large Quantum Efficiency Enhancement in Conjugated Macromolecules Induced by Extreme Deformations from Interfacial Friction of Dewetting", Master thesis 2010, Department of Materials Science and Engineering, National Tsing Hua University.
[13] P.-T. Chen, A. C.-M. Yang, "Optical Behavior of the Conjugated Polymer MEH-PPV Thin Films Stretched in Bi-Layer Dewetting by An Unstable Layer", 2012 March Meeting of American Physical Society (B48-13), Boston, MA, U.S.A, manuscript in preparation.
[14] M. Yan, L. J. Rotherberg, E. W. Kwock, and T. M. Miller, *Phys. Rev. Lett.* **75**, 1992 (1995).
[15] J.-L. Bredas, J. Cornil, D. Beljonne, D. A. Dos Santos, and Z. Shuai, *Acc. Chem. Res.* **32**, 267 (1999).
[16] Z. An, C. Q. Wu, and X. Sun, *Phys. Rev. Lett.* **93**, 216407-1 (2004).
[17] T. Drori, et al., *Phys. Rev. B* **76**, 033203 (2007).
[18] M. Fox, *Optical Properties of Solids*, Oxford University Press, 2001.
[19] Y. Chien, Y.-L. Chang, P. Lee, T. L. Lin, A. C.-M. Yang, "Molecular Stresses and Packing in Ultrathin Polymer Films from Spin Casting", in submission; Y. L. Chang, *Master Thesis* 2008, Department of Materials Science and Engineering, National Tsing Hua University, Taiwan.
[20] G. Reiter, M. Hamieh, P. Damman, S. Sclavons, S. Gabriele, T. Vilmin, and E. Raphael, *Nat. Mater.* **4**, 754 (2005).
[21] M. H. Yang, S. Y. Hou, Y. L. Chang, A. C.-M. Yang, *Phys. Rev. Lett.* **96**, 066105 (2006).
[22] S. Al Akhrass, G. Reiter, S. Y. Hou, M. H. Yang, Y. L. Chang, F. C. Chang, C.F. Wang, A.C.-M. Yang, *Phys. Rev. Lett.* **100**, 178301 (2008).
[23] P. Lee, Y. Chien, T.-L. Lin, A. C.-M. Yang, "Residual Stress Effects on Photoluminescence Efficiencies of Conjugated Polymer Confined in Thin Films", in preparation.
[24] G. Reiter, *Phys. Rev. Lett.* **68**, 75 (1992).
[25] A. Sharma, and G. Reiter, *J. Coll. Interf. Sci.* **178**, 383 (1996).
[26] P.-G. de Gennes, F. Brochard-Wyart, and D. Quere, *Capillarity and Wetting Pnomena :Drops, Bubbles, Pearls, Waves*, New York, Springer (2004).
[27] R. Seemann, S. Herminghaus, and K. Jacobs, *Phys. Rev. Lett.*, **86**, 5534 (2001).
[28] A. Nelson, *J. App. Cryst.*, **39**, 273 (2006).
[29] O. S. Heavens, *Optical Properties of Thin Films*, Butterworth, London, 1955.
[30] J. Liu, T.-F. Guo, Y. Yang, *J. App. Phys.*, **91**, 1595 (2002).
[31] P. Muller-Buschbaum, P. Vanhoorne, V. Scheumann, and M. Stamm, Europhys. Lett. 40, 655 (1997).
[32] T.-M. Huang, J.-Y. Lin, A. P. Le, O. Marin, C.-N. Liao, A. C.-M. Yang, "Ultra-Low Electric Resistivity of Conjugated Polymers Confined in Mesoscopic Thin Films", in submission.
[33] M. Geoghegan, C. Wang, N. Rehse, R. Magerle, G. Krausch, *J. Phys.: Condens. Matter* 17, S389 (2005).

Appendix:

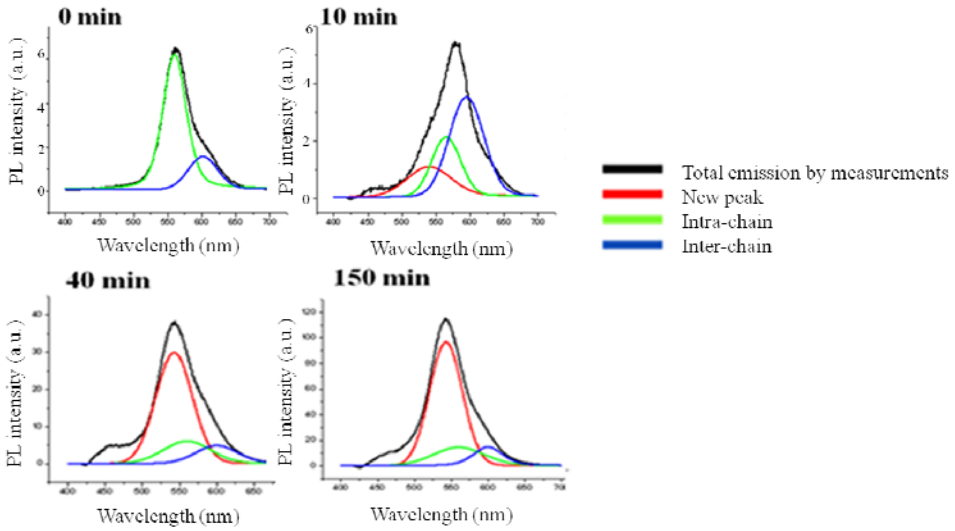

Evolution of the PL spectrum of 20 nm MEH-PPV/PS on bare silicon, silica, and PDMS-coated bare silicon, and the emission intensities of the resolved peaks (of Fig. 3a) and the residual layer area fraction versus dewetting time in a typical sample of 25% MEH-PPV ($\tau = 20$nm).

4. Optical behavior of the conjugated polymer MEH-PPV thin films stretched in bi-layer dwetting by an unstable layer

Molecular packing and chain conformation play important roles in the optoelectronic performance of conjugated polymer thin films. It has been shown that by virtue of stretching via dewetting, the photoluminescence (PL) efficiencies of rarefied MEH-PPV thin films may be dramatically enhanced. To result similar effects in the stable non-diluted pristine MEH-PPV thin films, bi-layer dewetting was attempted in samples of MEH-PPV thin films (~7nm) covered by one layer of polystyrene (PS) (~40nm) that dewetted in toluene vapor to form droplets (height ~300 nm) and ultrathin residual layer (~3nm) on the substrate. The instability was initiated from the PS layer in which small pinholes first emerged upon the intake of the solvent vapor. The pinholes then expanded and deepened into the underlying MEH-PPV, forcing the conjugated film to dewet. As a result of the stretching induced by the dewetting, the PL peak blue-shifted 20 nm to 540 nm and the intensity was enhanced around 10 times. Revealed by the position-sensitive confocal PL data, the huge enhancement came from both the droplet and residual layer, caused by molecular separation and stretching. Electroluminescence devices are being made based on these stretched MEH-PPV films.

Introduction

The PLED and polymer solar cell are valuable for energy crisis, because of low cost, easy process, flexible and environment friendly. The efficiency of devices is affected by mobility, band gap and optical character[1.2.3.4.] of polymer. The molecular packing and molecular conformation play the important role in polymer optical and electric character. Recently we stretched the conjugated polymer MEH-PPV by local deformation zones of the glassy polymer polystyrene, and then a dramatic increase of photoluminescence efficiency was resulted[5.]. This stretching-induced PL enhancement was attributed to the suppression of electron-phonon coupling of the stress-rigidified chains[5.]. This experiment clearly elucidates the close dependence of optoelectronic behavior of conjugated polymers on the mechanical

properties. Separately, we found that when an ultrathin polymer films that containing MEH-PPV molecules underwent dewetting, a very large enhancement was also observed[6]. After careful examination, this effect was arising from the stretching of the conjugated polymer during the long distance flow of polymer that formed the droplets and a thin residual layer on the substrate. This experiment was on the ultrathin films containing of ~20% of MEH-PPV in polystyrene. Since pristine MEH-PPV films are used for most applications, we were trying to observe this dewetting-induced enhancement in pure MEH-PPV films. However, even the ultrathin, ~7nm thick, pure MEH-PPV thin films won't dewet at a high temperature or in an solvent vapor bath. Only local aggregation of polymer chains that caused red-shift was observed (S. 1 and 2). This indicates that the polymer strength of the pure MEH-PPV ultrathin films is greater than that of the residual stress and capillary forces combined[7-9]. Thus, we were trying to add an additional driving force to trigger the instability of the pure MEH-PPV films by stacking an ultrathin PS film on top of it and annealing the bi-layers to induce dewetting. There is a large residual stress stored in the PS layer. Now this advantage of dewetting process will be tried to use in PLED or PV device.

Experimental Methods

Generally, a PS film (Mw = 200,000 g/mol., DPI ≤ 1.05), was used as upper layer. And the bottom layer is MEH-PPV purchased (Mw = 40,000-70,000 g/mol.) from Sigma-Aldrich Chemical Co. Thin PS film (thickness ~40nmm) were prepared by spin casting on clean glass from the polymer solution in toluene. The film was subsequently floated off on a water surface and transferred onto MEH-PPV layer spun on Si wafer by using MEH-PPV solution in a solvent of equal-parted toluene, tetrahydrofuran, and cyclohexanone. After drying, we solvent-annealed it by toluene at 30C to trigger the dewetting.

The PL spectra were measured by spectrometer (Horiba-Jobin Yvon nanolog) excited at a relatively low wavelength 350 nm for reduced background noises.

The topography and microstructure of the samples were studied using optical microscope (Nikon Eclipse LV1000PDL) and the depth profile was measured by time-of-flight secondary ion mass spectrometer .A confocal PL was used to explore the microscopic luminescent properties of the samples.

Results

In this bi-layer structure, we observed that dewetting was successfully triggered (Fig. 1), as shown here where a 7 nm MEH-PPV film and 40 nm PS film were put together and used. In this case, for approximately 30 minutes in solvent vapor pinholes appeared. They subsequently developed into large holes, connected together, and finally evolving into droplets. The average diameter of the droplets is about 20~30um, the height is about 300 to 500 nm, and the thickness of the residual film is around 3.5 nm.

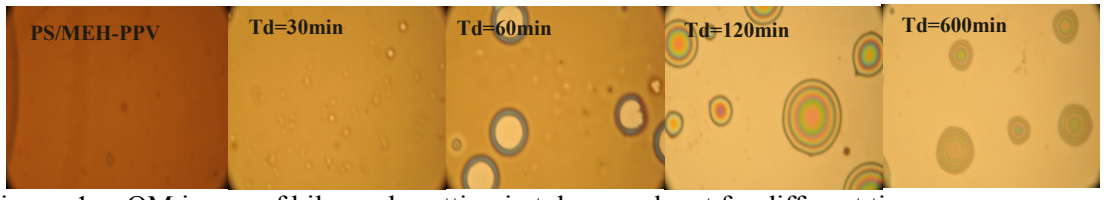

Figure 1. OM image of bilayer dewetting in toluene solvent for different time.

During the dewetting, the PL intensity was observed to increase dramatically with a clear blue shift. (Fig.2)For the sake of analysis, the PL spectrum was separated into three Gaussian components: the traditionally attributed intra-chain emission (at ~570 nm) and inter-chain emission (at ~605nm) [10.11.], as well as a dominating new peak due to dewetting located at 543 nm (Fig. 3). It is important to note that for this case the enhancement started

very early at 30 nm when only pinholes emerged and the enhancement at this point was approximately 10 times and increased only slightly later on during the dewetting.

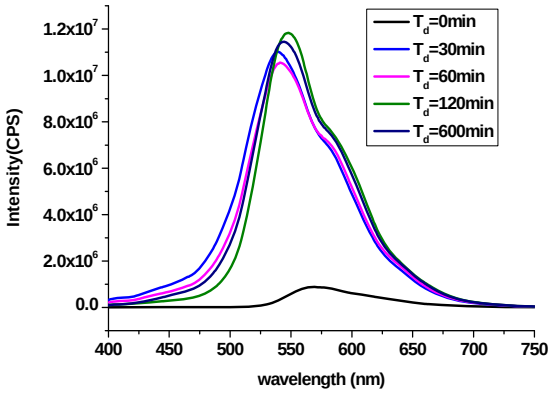

Figure 2. PL measurement of bilayer structure build form 2nm MEH-PPV and 40 nm PS.

In comparison, when the thickness of MEH-PPV film increased to 23 nm and 35 nm, the enhancement decreased and delayed. Nevertheless, the final enhancements for these thicker MEH-PPV films still ran at about 2 times and 40% respectively. (Fig.4)
We also noted that in the cases of thicker MEH-PPV film, the new peak was not as dominating as that in the case of thin 7 nm film, indicating that the dewetting effect in fact was smaller in the thicker MEH-PPV films.

To understand this thickness effect, we know that the residual stress decreased quickly with film thickness. The long-range van der Waals interactions also decreased with the square of the film thickness. Thus, for thicker MEH-PPV films, the stretching force during dewetting was apparently much less than that in the thin 7 nm film, thus giving rise to much smaller dewetting-induced enhancement.
On the other hand, the capillary force dominates in the droplet formation and the theory pred icts the existence of an residual layer at a thickness of h*. For the residual layer thickness of around 3.5 nm, the chains of the 7nm film were more restricted by the substrate adhesion dur ing dewetting.

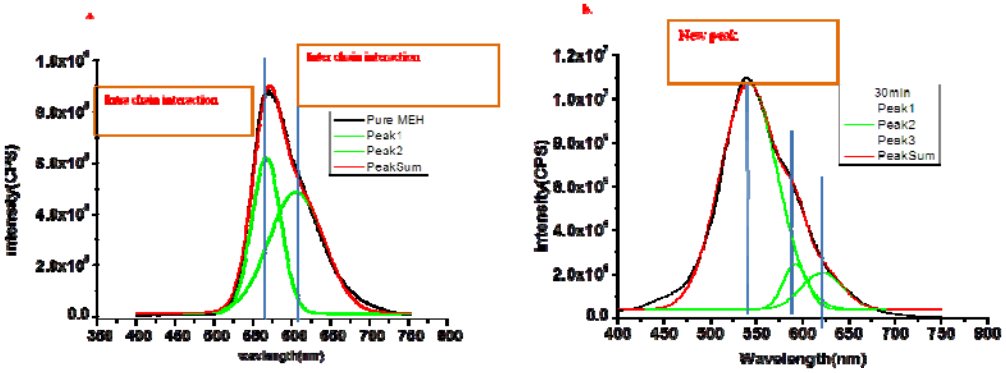

Figure 3. Gaussian fitting for a. pure MEH-PPV b. for dewetting film.

When the PS thickness was varied to thicker films, the dewetting enhancement increased. We attribute this effect to the increase of the stretching force from PS for which the force is the product of residual stress and the film thickness, and increased with the film thickness. (Figu re 5)

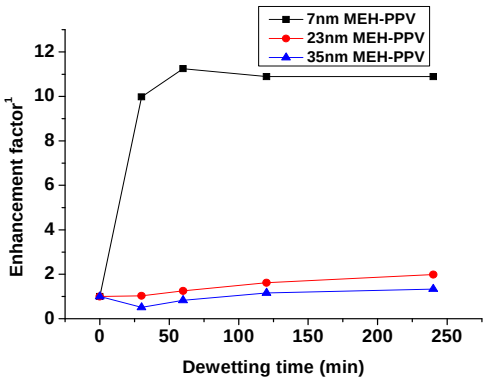

Figure 4. PL enhancement of bilayer dewetting for different thickness of MEH-PPV
Enchantment factor = new peak intensity/ peak intensity of pristine MEH-PPV

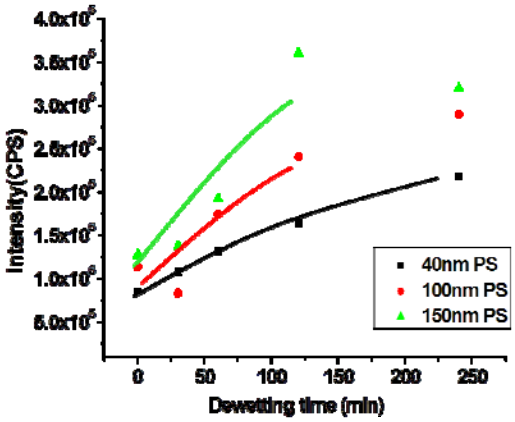

Figure 5. PL intensity of new peak in bilayer dewetting for different thickness of PS

To further reveal the molecular movement during the two-layer dewetting, the depth profiles of the droplets were analyzed by using time-of-flight secondary ion mass spectrometer (SIMS). We found that the depth concentration profile of the MEH-PPV was constant with depth, indicating uniform intermixing between the MEH-PPV and PS during the dewetting. (Fig. 6)

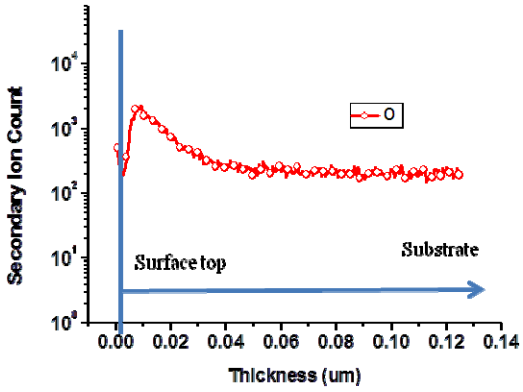

Figure 6. Oxygen signal of SIMS form bilayer dewetting

On the other hand, using the confocal micro-PL spectrometer the residual layer emitted light more efficiently without significant spectral shifts relative to the non-dewetted MEH-PPV

films, a behavior very similar to that reported in simple stretching[6]. It also indicates that the residual film was mostly pure MEH-PPV. On the droplets, however, the PL enhancement was considerably larger than in the residual layer and a clear blue shift was detected. This indicates that the droplets was formed by stretching the intermixed MEH-PPV and PS (Fig. 7).It implies that interface intermixing of MEH-PPV and PS at the film interface preceded the dewetting. Furthermore, during the intermixing, residual stresses from both films were released to initiate molecular chain stretching that subsequently led to large scale material flows. As shown by the data of the thin 7 nm, the stress-induced optical enhancement had already induced by the molecular deformation on scales comparable to this stress release, estimated to be similar to the spacing between chain entanglement points (~3-10 nm). The subsequent material flows, that happened on a scale much greater than the previous molecular motions, only provided the renewal opportunity for this intermixing, stress release, and chain stretching processes, and then increasing the volume of stretched chains. For the very thin films where the restriction of substrate friction is important, it is difficult for the material flows to generate further volume increase of the stretched chains, such as the case of the 7 nm MEH-PPV where the enhancement was almost saturated when the pinholes emerged.

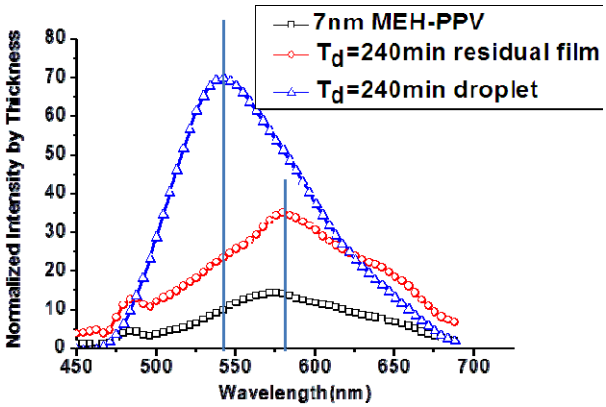

Figure 7. Confocal PL of bilayer dewetting

The OLED device behavior of bilayer system is almost the same as control device (pure MEH-PPV) (Table1). According the result of multilayer dewetting(Fig.13) the multilayer dewetting is finished after 1 hour. Compared IV spectrum the pure and dewetting device, the slope is almost the same (Fig.8). The charges are transferred by the MEH-PPV. The turn-on voltage is increase in multilayer dewetting device because covered PS makes band gap become larger. In the EL spectrum the interchain interaction became clear and the intrachain interaction also show redshift (Fig.18). The solvent would make the aggregation of MEHPPV film. The redshift behavior is the same as confocal PL data of residual layer. These imply the charge like to transport and recombination in residual layer. Although the efficiency of dewetting sample is almost the same as the control device, the thickness and area of the active layer (residual layer) is smaller. The experiment still needs to be improved. Because process of covered PS is though water. But water would make device fail easily. So substitution of water is key for this experiment.

	Yield(cd/A)	Luminance Eff(lm/watt)	Luminance(cd/m^2)	V
Pure MEHPPV	3.74E-01	1.07E-01	4.56E+02	11V

Dewetting (T_d=180min)	3.21E-01	1.32E-01	3.79E+02	11V

Table.1 device performance of bilayer system

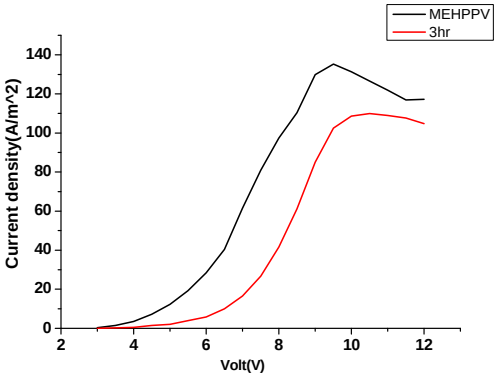

Figure 8. The IV curve of bilayer system.

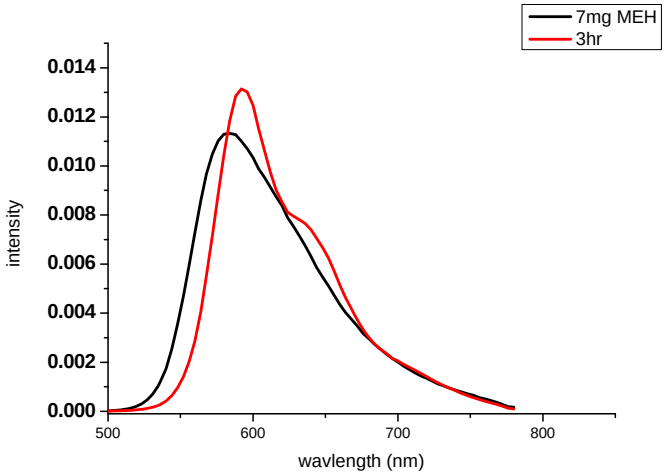

Figure 9. The EL spectrum of bilayer dewetting system

References

1. J. Phys. Chem. 100, 12532(1996), Raman Spectroscopic Studies of Regioregular Poly(3-alkylthiophenes)
2. C. Goh, J. Kline, M. D. McGehee, E. N. Kadnikova, M. J. Fre´chet Appl. Phys. Lett. 2005, 86, 122110.
3. Y. D. Park, D. H. Kim, J. A. Lim, J. H. Cho, Y. Jang, W. H. Lee ,J. H. Park, K. Cho, J. Phys. Chem. 2008
4. M. C. Scharber, D. Mu¨ hlbacher, M. Koppe, P. Denk, C. Waldauf A. J. Heeger, C. J. Brabec, Adv.Mater. 2006, 18, 789.
5. Tung, KP et,al, ACS NANO 2011, 5, 7296-7302.
6. R. Seemann, S. Herminghaus and K. Jacobs, Phys. Rev. Lett., 86, 5534–5537 (2001).
7. A. Sharma, Langmuir, 9, 861 (1993).
8. A. Sharma, Langmuir, 9, 3580 (1993).
9. E. Collini, G. D. Scholes, Science, 323, 369-373 (2009)

10. B. J. Schwartz, Annu. Rev. Phys. Chem., 54, 141-172 (2003).

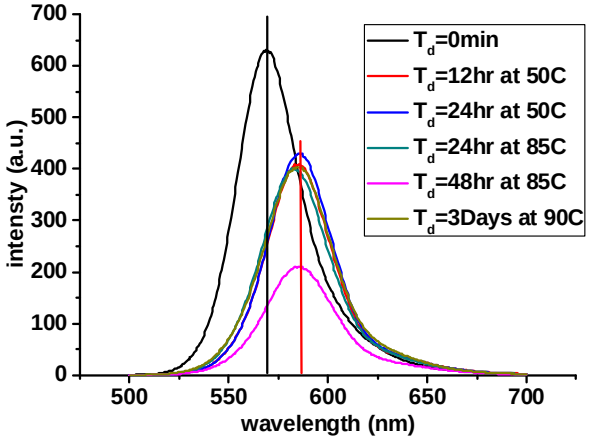

S. 1 PL spectrum of thin film after thermal and solvent annealing on the Si wafer

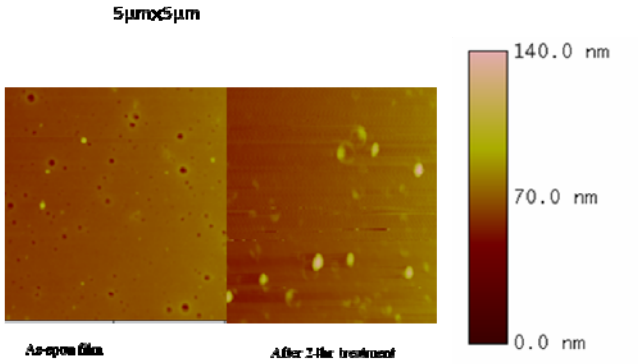

S. 2 AFM image of thin film after thermal and solvent annealing on the Si wafer

5. Crystallizing Conjugated Polymer Chains of P3HT Stretched for Dramatic Enhancements in Optoelectronic Efficiencies

Previously the amorphous conjugated polymer MEH-PPV was shown to illustrate huge enhancement in photoluminescence (PL) efficiencies upon stretching to large molecular strai ns. In this work the crystallizing polymer of poly(3-hexylthiophene)(P3HT), dispersed in the polystyrene (PS) matrix, was stretched in the PS local deformation zones to study the effect o f molecular deformation. A huge enhancement of the PL intensity was observed that when no rmalized to the fraction of the strained polymer corresponded to an increase of 15 folds, signi ficantly larger than that of the stretched MEH-PPV. Moreover, when examined under a con-f ocal micro-PL (spot size ~5μm), the emission from the local deformation zones subject to a h igh stress (~40MPa) manifested marked increase of the intrachain emission relative to the eff ect on the interchain. These emission peak positions, however, were unaffected by the stretch ing. The PL enhancements were attributed to the depression of electron-phonon interactions

of the stretched P3HT chains. Constraining conjugated polymers to yield high efficiencies th us may provide a feasible way for improving the performance of polymer-based devices.

Introduction

P3HT is one of the most promising semiconducting conjugated polymers researched rigorously as an active layer in the polymer-based devices for higher optoelectronic efficiencies. Although the pristine P3HT molecules exhibit greater optoelectronic efficiencies compared to other conjugated polymers, the low quantum efficiency still impedes the practical realization of the organic devices. Various efforts have been attempted to improve the quantum efficiency of conjugated polymers in different environments while the basic factors responsible for the lower efficiency have not been resolved yet. Recently, we have demonstrated that by stretching the conjugated polymer MEH-PPV, a dramatic increase of photoluminescence (PL) efficiencies may be resulted. The efficiency enhancement was attributed to stretching of the polymer chains such that the electron-phonon interactions were suppressed. The dependence on the local stress in the stretched samples as well as the corresponding effect on the chain vibrations via Raman scattering were left unexplored.

Here, in this letter, we continue investigating this important topic by exploring the stretching-induced PL enhancement of P3HT, which is crystallizing, in comparison to that of the amorphous MEH-PPV. It was with the consideration that the self-assembly behavior of the molecular segments influences strongly the molecular packing in the thin films and thus the PL behavior; so does the mechanical stretching effect. The polymer P3HT is highly attractive due to its high electric conductivity and has been studied extensively for an active material role in solar cells as well as other polymer-based devices. The stress effect on P3HT would not only provide important information to unveil the mechano-optoelectronic effect for conjugated polymers in general but also shed important light for understanding and the proper exploitation of P3HT.

As unveiled by the experiments, we observed even greater PL enhancements in the stretched crystallizable chains of P3HT compared to the amorphous MEH-PPV. By examining the stress states of the stretched P3HT during the local deformation process, a clear correlation between the PL enhancements and the local stress was obtained, indicating that state of chain constraint indeed directly related to the level of the PL enhancement, consistent with the proposed mechanism of stress-rigidified chains where trapping of excitons reduced dramatically to give rise to greatly enhanced recombination. Very importantly, amid the close correlation between the PL enhancement and the local stress, it was found that the small stresses that corresponded to elastic strains ~0.5% of the glassy polymers were producing significant PL enhancement of ~2.5 folds. This indicates that by controlling the residual stresses in the polymeric thin films employed in the solar cells or emitting diodes, the optoelectronic efficiencies may be improved significantly. In addition, it was found that molecular stretching that produced large PL enhancement did not come with alternations of the Raman absorption peaks although the Raman intensities increased substantially. It clearly reveals that for PL enhancements changes of the vibration spring constant are not required, rather, it is the way how the local molecular strains are accumulated by the chain vibrations (or rotations) directly dictates how the PL is enhanced. Obviously, with the energy dissipation reduced dramatically by the molecular constraints, the enhancement of the optoelectronic efficiencies by mechanical stresses may be exploited for high efficiency polymer-based devices for light emitting diodes as well as solar cells.

Experimental Procedures

We use a high molecular weight polystyrene (PS), PS2M (Mw= 2,000,000 g/mol., DPI $\leq$ 1.3), as the matrices, and blending with conjugated polymer, poly(3-hexylthiophene) (P3HT) (Mw= 5,500 g/mol., DPI $\leq$ 2) were purchased from Luminescence Chemical Engineering Technology Ltd.

The solvent is toluene, and substrate for spin coating is glass. After the solvent and polymer well mixing, filtrating by the 0.45 μm filter. The polymer solution was spin-coated on glass and put it in water. The film (thickness is 0.5μm) was floated off on water surface and transferred onto a piece of copper grids. Samples were put in the glove box for 24hr until the solvent evaporated completely and stretched uni-axially on a strain jig after the solvent vapor treatment for enhanced bonding to the copper grid.

We compared the photoluminescence spectra by photoluminescence spectrometer (Horiba Jobin Yvon Fluorolog-3) and the morphology of polymer film by atomic force microscope (AFM, Digital Instrumental, Nanoscope IIIa and Dimension^{TM} 3100). Moreover, we see the micro structure of those deformation zones by Transmission electron microscopy (TEM, JEM-2100(HT) 200KV Electron Microscope (LaB_6) with 3D Tomography).

Results and Discussions

Upon stretching, the film containing P3HT developed crazes (Fig.1a). The population of the crazes initially increased with the external strain *e* linearly but soon leveled off as the applied strain became greater than ~4.0% (Fig. 1b). It indicates that craze widening was the major contribution to the material extension for e > ~4.0% while for e < 4.0% craze nucleation was the dominant mechanism for sample extension. From the AFM topography of these crazes (Fig. 1c), craze depth versus craze width, a behavior very similar to the mechanical "necking" was observed. As the concentration of P3HT increased, the craze depth decreased (Fig. 1c), indicating that the dispersed P3HT had participated in the drawing of the crazes.

Since the stretching of the polymer into crazes follows a necking process, the local stress and strain distributions inside the crazes can be obtained by using the Bridgman's necking theory for plastic deformations.[8-10] Following the Bridgman plastic necking theory, the local drawing stress parallel to the stretching direction $_z$ is given as

$$\sigma_z = F\left[1+\log\left(\frac{\phi^2+2\phi R-r^2}{2\phi R}\right)\right]$$

where F is the drawing tension force, and R are respectively the local thickness and radius of curvature at the neck, h is the film thickness outside the neck, and E is the Young's modulus of the film.

a) b)

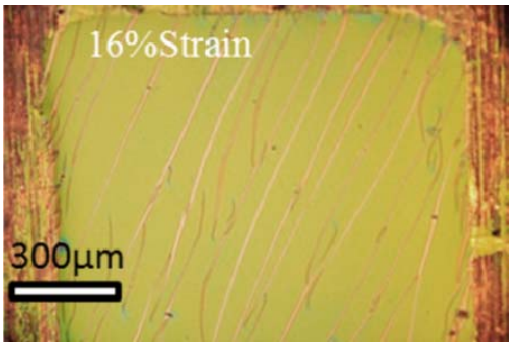

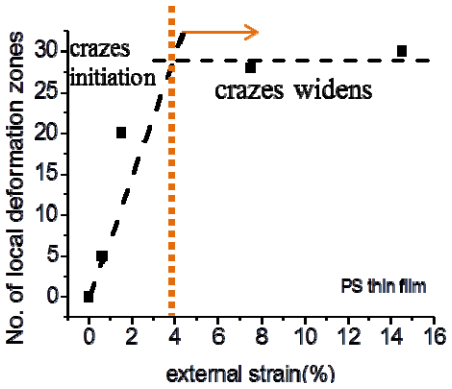

c)

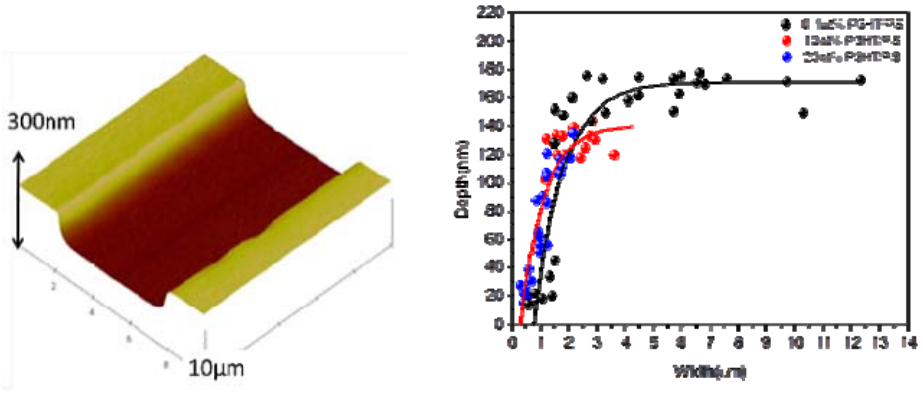

Fig.1 (a) The optical microscope image of 0.1 wt% P3HT with 16% external strain. (b) The t opography of craze. b) The number of local deformation zones with various external strain. c) the necking topography revealed by the AFM and the correlation between the craze width a nd craze depth that indicated necking is operative during crazing.

The tensile stress σ_t and true strain ε, on the other hand, are given as

$$\sigma_t = \frac{\beta}{hw} F = \frac{E\varepsilon_c h_0}{h}\beta, \qquad \varepsilon = \ln\left(\frac{h_0}{h}\right) - \frac{1}{3}\ln v_f + \varepsilon_c$$

where v_f is the volume fraction of polymer in the craze, ε_c is the critical strain for crazing, and β is a correcting geometric factor. In the typical distribution of stress inside a craze, the averag e stress is around 70 MPa (Fig.3). Cross plot the local stress and strain gave the stress-strain curve for craze drawing. In films of low P3HT concentrations, the crazes were generally well developed and the local stresses inside the crazes are much higher than that in films of more concentrated P3HT. Poorly fibrillated P3HT aggregates were observed in concentrated sam ples.

(a)

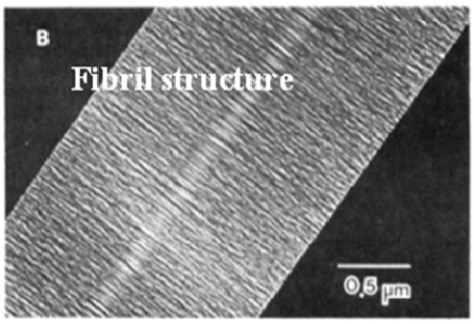

(b) (c)

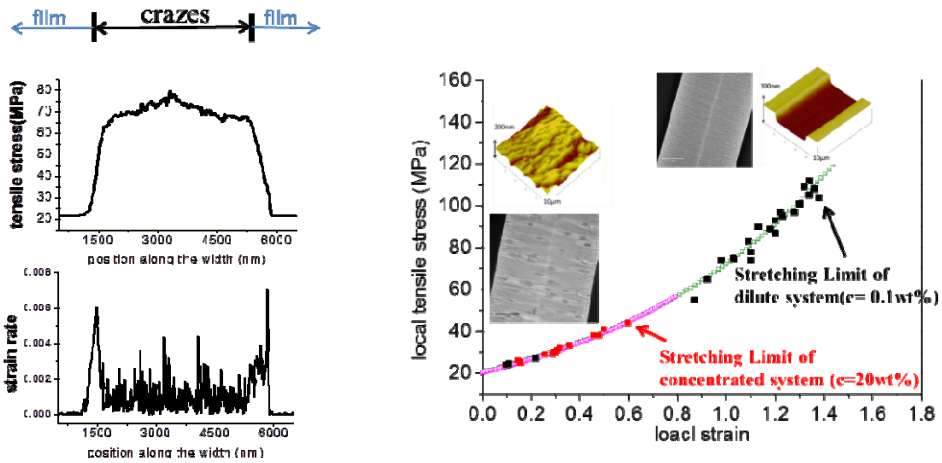

Figure 2. a) The TEM fibril structure of the craze, b) The local stress and strain in the crazes distribution, and c) The local tensile stress and local strain in the crazes.

We found that, for low P3HT concentrations, the PL enhanced with the deformation. The enhancement, however, decreased as the P3HT concentration increased. It clearly indicates that, in addition to the P3HT aggregation effect, the PL enhancement increased with local tensile stresses.

a)

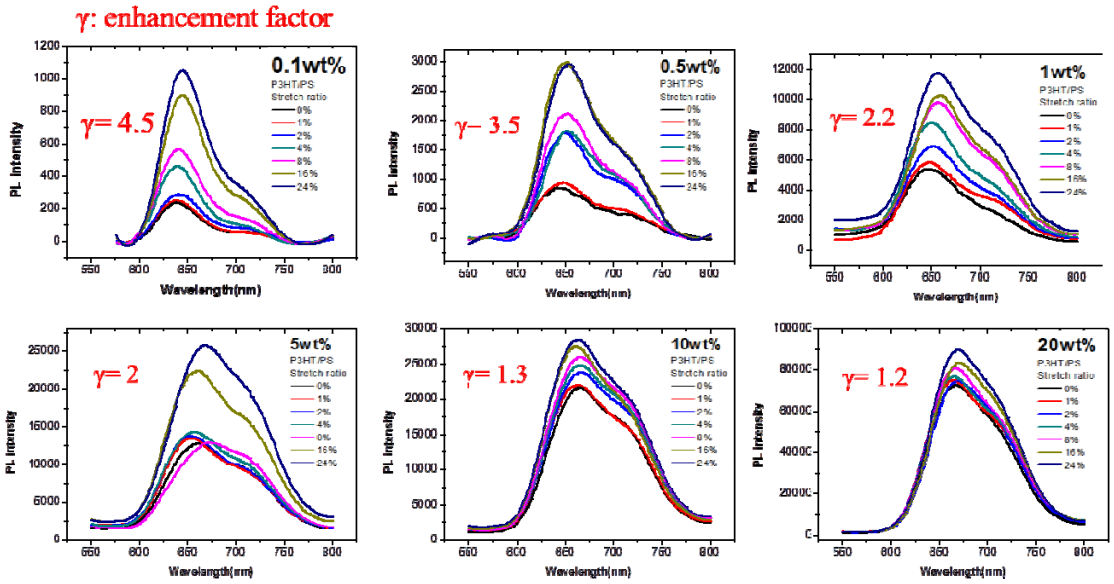

b) c)

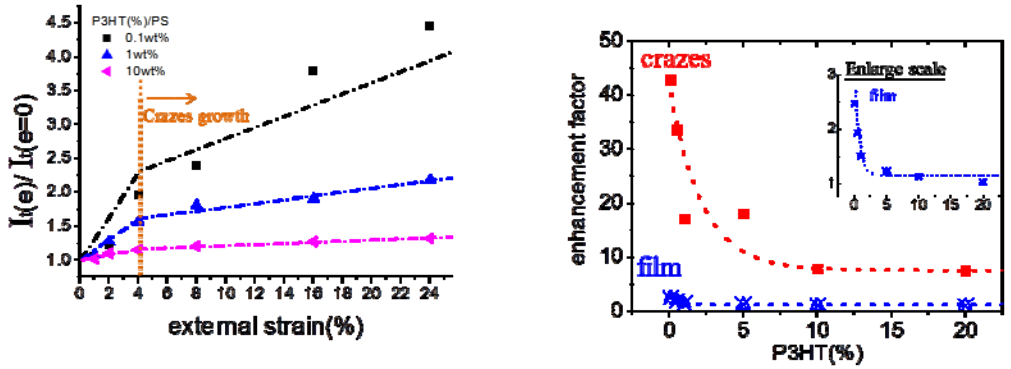

Figure 3. a) The PL enhancements of various concentration of P3HT. b) The relative PL

intensity with various external strains. c) The enhancement factor of crazes and film of different P3HT concentrations.

To quantitatively analyze the PL data, we further assumed that the total PL (I_t) came from the crazes (I_c) and the regions outside the crazes (I_f), i.e., $I_t(e) = I_f(e) + I_c(e) = i_f wh_0 l(1-e_p) + i_c whle_p\theta_c$ where i_f and i_c are respectively the PL per unit volume from the regions outside the crazes and that from the crazes, e is the applied strain, $e_p = e - \varepsilon_c$ is the plastic strain applied to the sample, w and l are respectively the width and length of the sample, h_0 and h are respectively the thickness of the region outside the crazes and the thickness within crazes, and θ_c is the fibril packing density in crazes usually assumed to be 0.8 for the closest packing of cylinders. From this relationship, the total PL (I_t) normalized to that before stretching ($I_{t,0}$) can be readily derived as

$$\frac{I_t(e)}{I_t(e=0)} = \frac{i_f(e)}{i_f(e=0)} + \left(\frac{i_c(e)}{i_c(e=0)\lambda_c} - \frac{i_f(e)}{i_f(e=0)} \right) e_p ,$$

where we have used the relationship that the draw ratio of the craze fibril $\lambda_c = 1/\nu_c = h_0/h\theta_c$. From the expression of $I_t/I_{t,0}$, the PL enhancements in the region outside the crazes ($\xi_f = i_f/i_{f,0}$), and inside the crazes ($\xi_c = i_c/i_{c,0}$), can be obtained from the behavior of the total PL (I_t), normalized to that before stretching ($I_{t,0}$), as a function of the applied plastic strain e_p. Such data were plotted in Fig. 3b for various P3HT concentrations where straight lines evidently provide reasonable fit. In fact, for each sample the enhancement factors in both the stressed polymer outside the crazes and that inside were constant because the local strain outside the crazes was approximately fixed at $e = \varepsilon_c = 0.5\%$ while that inside the crazes was pinned at ($\varepsilon_c \lambda_c$ -1), independent of the applied strain (e). Thus, the enhancement factors ξ_f and ξ_c were obtained from the intercept and the slope, respectively, of the linear fit.

a) b)

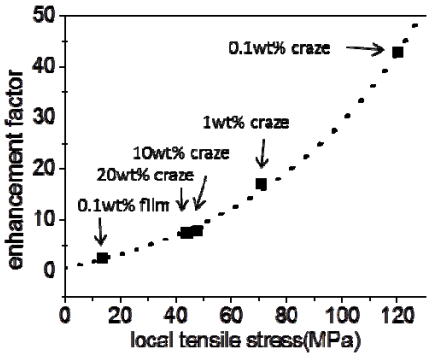

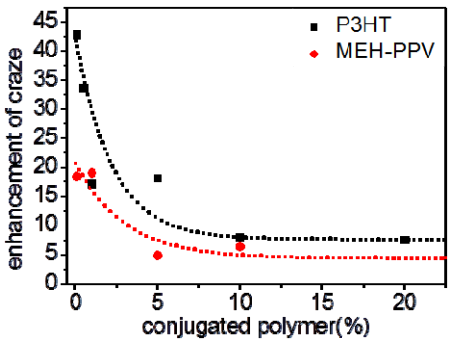

(c)

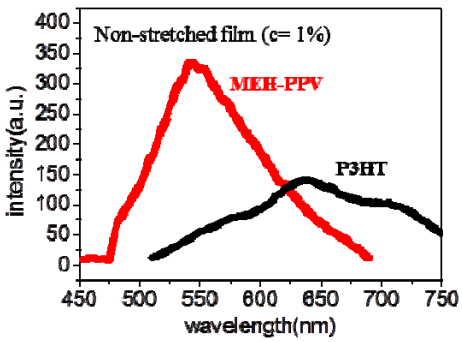

Figure 4. a) The enhancement factor with different local tensile stress. b) The enhancement factor of P3HT and MEH-PPV, c) Their pristine PL intensity. d) The Raman spectra of P3HT and MEH-PPV within and outside the crazes.

After doing that, we found the enhancement factor for the P3HT stretched in the crazes can go up to around 40 times (Fig.7). As the P3HT concentration increased, the enhancement decreased along with the decrease of local stresses. In the film regions, however, the stretch-induced PL enhancement was much smaller, running from 2.5 times, for the dilute samples, to 1.0, for the concentrated ones although the local stress was approximately the same. This indicates that in order to have the stress-enhanced effect, the deformation incurred has to be on the molecular level. For aggregates in the concentrated samples, it was very difficult to break up the molecules for molecular stretching, hence very small or even no enhancement could be resulted by stresses.

Finally, we compare the stretching effect on P3HT with that of MEH-PPV. We found that the enhancement was much greater for P3HT. For the 0.1% concentration, the enhancement is about 43 folds for P3HT versus 17 folds for MEH-PPV (Fig.8). This difference may be due to the lower PL efficiencies of the non-stretched P3HT in comparison to the MEH-PPV, which may be related to the crystallizable chain nature of the P3HT.

Conclusions

Tensile stresses may give rise to great enhancement in the optoelectronic efficiencies of P3HT polymers. The stress-induced enhancement has to be accompanied with the deformations on the molecular levels. The stress-induced enhancement is greater in P3HT compared to MEH-PPV.

Acknowledgments:

We greatly appreciate the inspiring discussions with Günter Reiter of the University of Freiburg, Germany. We also thank the financial supports by the National Science Council of Taiwan and the US Air Force Office of Scientific Research through the Taiwan–US Air Force Nanoscience Initiative Program (AOARD-094024, -104055, and -114055).

References

1. J. Shinar and J. Partee, Syn. Met., 1997, 84, 525-528
2. L. J. Rothberg, M. Yan, S. Son, and etc., Syn. Met., 1996, 78, 213-216.
3. K.-P. Tung, and etc, ACS Nano, 2011, 5 (9), 7296–7302
4. L. L. Berger and E. J. Kramer, Macromolecules 1987,20, 1980-1985
5. C. Y. Hui, A. Ruina, C. Creton, and E. J. Kramer, Macromolecules 1992,25, 3948-3955
6. T. N. Krupenkin and G. H. Fredrickson, Macromolecules 1999, 32, 5029 – 5035
7. H.-H. Kausch, Crazing in Polymers. Vol. 2, 1990
8. P. W. Bridgman Studies in Large Plastic Flow and Fracture, Cambridge, p. 9(1964)
9. G'sell C.; Marquez-Lucero A. Polymer, 1993, 34, 2740.
10. A. C.-M. Yang, and etc., Macromolecules 1993, 26, 1767.

List of Publications:

1. Kuang-Po Tung, Chein-Chung Chen, Peiwei Lee, Yi-Wei Liu, Tzay-Ming Hong, Kuo Chu Hwang, Jui-Hung Hsu, Jonathan David White, Arnold C.-M. Yang, **2011**, "Large Enhancements in Optoelectronic Efficiencies of Nano-plastically Stressed Conjugated Polymer Strands", *ACS Nano* 5, 7296.
2. Anh Phuong Le, Tsai-Ming Huang, Po-Tsun Chen, Arnold C.-M. Yang, **2011**, "Synthesis and Optoelectronic Behavior of Conjugated Polymer Poly(3-hexylthiophene) Grafted on Multiwalled Carbon Nanotubes", *Journal of Polymer Science Part*

B-Polymer Physics 49, 581.
3. Chun-Chih Chang, Yi-Hsin Chang, Kuo-Chu Hwang, Jwo-Huei Jou, Arnold C. -M.Yang, **2011**, "One-step Fabrication of pi-Conjugated Polymer Thin Films from Naphthalenes via Plasma Polymerization for Efficient Optoelectronic Devices: White Polymer Light-emitting Diodes", *Plasma Processes and Polymers* 8, 215.
4. C.-C. Chang, L.-W. Wang, Y.-H. Chen, K.-C. Hwang, J.-H. Jou, Y.-S. Chang, A. C.-M. Yang, **2012**, "White Luminescent Polymers by Plasma Polymerized Iridium Complexes from 1,10-Phenanthroline", *Plasma Process. Polym.* **9**, 225.
5. Chih-Wei Lin, Steve L.-C. Hsu, Arnold C.-M. Yang, **2012**, "Micro-Drawing of Glassy Polybenzoxazole Rigid Rods and the Molecular Interactions with Carbon Nanotubes", *Polymer* **53**, 1951.
6. Tsai-Ming Huang, Jin-You Lin, Le Anh Phuong, Orlando Marin, Chien-Neng Liao, Wha-Tzong Whang, Arnold C. -M. Yang, **2012**, "Ultra-Low Resistivity of Charge Transport in Ultrathin Polymer Films", in submission.
7. P. W. Lee, W. C. Li, B. J. Chen, G. Reiter, C. W. Yang, C. C. Chang, C. T. Yuan, J. Tang, T. L. Lin, P. K. Wei, A. C.-M. Yang, **2012**, "Massive Enhancement of Photoluminescence of Conjugated Macromolecules Induced by Dewetting", in submission.
8. Y. L. Chang, Y. CHIEN, A. C.-Y. Chou, G. Reiter, A. C.-M. Yang, **2012**, "Molecular Packing of Long Polymer Chains in Ultrathin Films via Spin Casting", in submission.
9. Chen, C. C.; Chen, B. T.; Yang, A. C.-M., "Method for Enhancing Luminescent and Power Generation Properties of Conjugated Polymers", filed for Patent application, **2011**, Taiwan and US (12/571,110).

DD882 as a separate document was complete.